POST-PRINT

High-resolution stratigraphy and chronology of seven distal, Campanian-derived tephra layers interbedded with varved sediments aged 40-38 cal ka BP in Lago Grande di Monticchio: local impacts, re-mobilisation, and implications for palaeoenvironmental reconstruction

Kristina Wutke [1,2], Sabine Wulf [2*], Emma L. Tomlinson [3], Mark Hardiman [4,5], Peter Dulski [2], Jürg Luterbacher [1] and Achim Brauer [2]

[1] Department of Geography, Climatology, Climate Dynamics and Climate Change, Justus-Liebig University, Senckenbergstrasse 1, D-35390 Giessen, Germany
[2] Helmholtz Centre Potsdam, GFZ German Research Centre for Geosciences, Section 5.2 – Climate Dynamics and Landscape Evolution, Telegrafenberg, 14473 Potsdam, Germany
[3] Department of Geology, Trinity College Dublin, College Green, Dublin 2, Ireland
[4] Centre for Quaternary Research, Department of Geography, Royal Holloway University of London, Surrey TW20 0EX, United Kingdom
[5] Department of Geography, University of Portsmouth, Portsmouth, P01 3HE, United Kingdom

Abstract

We present the results of new tephrostratigraphical and environmental impact studies of the 40-38 ka varved sediment section of Lago Grande di Monticchio (southern Italy). The sediments in this time zone are correlated with the Heinrich H4-stadial that occurred between Greenland Interstadials GI-9 and GI-8, and include the widespread Campanian Ignimbrite (CI, 39.3 ka) as a thick tephra layer in the middle of the H4 stadial. The CI in the Monticchio record is overlain by the Schiava tephra from Vesuvius, c. 1240 varve-years younger than the CI, and preceded by four tephras from small-scale eruptions of the Phlegrean Fields and by an Ischia-derived tephra. The four Phlegrean Field-derived tephras were deposited 600 varve-years or fewer prior to the deposition of the CI and show very similar major, minor, and trace element glass compositions compared to those of the CI. This similarity in composition and age may lead to erroneous tephra identification and therefore potentially compromise the accurate linking and synchronisation of palaeoenvironmental records in the central Mediterranean area. Microfacies analyses and µ-XRF core scanning were used to characterise

Published in Quaternary Science Reviews.
http://www.sciencedirect.com/science/article/pii/S027737911400198X

primary and secondary depositional features of all seven tephra layers and to evaluate environmental and ecological responses after tephra deposition. Higher concentrations of tephra-derived material (mainly glass shards and pumices) in primary and reworked layers were detected by elevated K-counts in µ-XRF elemental core scans. Reworked tephra derives mainly from in-washing from the littoral zone and the catchment and occurs within five to 30 years, and up to 1240 varve years, after the deposition of thinner (1-5 mm) and thicker (5-230 mm) tephra fallout deposits, respectively. An obvious response of diatom population growth directly after the primary tephra deposition was observed for the thicker tephra layers (> 1 mm) during the first 1 to 8 years after deposition of the primary deposit indicating that the additional input of potential nutrients (glass shards) affected the ecological lake system.

Keywords: tephrochronology, Lago Grande di Monticchio, Campanian Ignimbrite, µ-XRF scanning, environmental impacts, reworked tephra

1. Introduction

The Mediterranean region is of special interest in terms of tephrostratigraphical study because of the long history of explosive volcanic activity (e.g., Keller et al., 1978; Narcisi and Vezzoli, 1999; Druitt et al., 1999; Peccerillo, 2005). During the Late Quaternary, the Roman Comagmatic Province with the Campanian volcanoes in southern Italy were influenced by very frequent and explosive volcanism creating numerous widespread tephras which are often preserved as primary fall deposits in terrestrial and marine sediments (e.g., Keller et al., 1978; Paterne et al., 1986, 1988; Narcisi, 1996; Narcisi and Vezzoli, 1999; Siani et al., 2004; Wulf et al., 2004, 2012; Munno and Petrosino, 2007). Over the last decade, numerous cryptotephra studies have added to the existing 300 ka distal tephrostratigraphy of the Italian volcanism (e.g., Lowe et al., 2007; Wulf et al., 2008; Bourne et al., 2010; Sulpizio et al., 2010). A key tephrostratigraphical record is the annually laminated lacustrine sediment repository of Lago Grande di Monticchio in southern Italy. This maar lake is located within 100 to 140 km and downwind of the Campanian volcanoes (Fig. 1), thus documenting the majority of explosive events from the Campanian volcanoes for the last 133 ka (Narcisi, 1996; Wulf et al., 2004, 2008, 2012). A total of 345 primary tephra layers have been deposited in context with high-resolution palaeoenvironmental information (e.g., Allen et al., 1999; Brauer et al., 2000, 2007) in the Monticchio sequence and are additionally well dated by the varve-supported sedimentation rate chronology of Monticchio sediments. So far, more than 30 tephra layers were precisely correlated with dated volcanic events and therefore provide important marker

layers for independently dating and correlating the Monticchio record with other terrestrial and marine palaeoclimate records in the Mediterranean (Wulf et al., 2004, 2008, 2012). One of these marker layers is the tephra labelled as TM-18 in the Monticchio record, a correlative of the basal fall unit of the Campanian Ignimbrite (CI), which erupted from the Campi Flegrei Caldera 39.28 ± 0.11 ka BP ($^{40}Ar/^{39}Ar$; De Vivo et al., 2001). The CI eruption was one of the most powerful known in the Mediterranean region for the last 200,000 years (Barberi et al., 1978), and distal deposits – correlated with the marine Y-5 tephra – are distributed mainly towards the east as far as Russia (e.g., Keller et al., 1978; Thunell et al., 1979; Paterne et al., 1988; Vezzoli, 1991; Pyle et al., 2006; Giaccio et al., 2008). The eruption of the CI occurred during marine isotope stage (MIS) 3, ca. 1600 yrs after the Laschamp geomagnetic excursion (41 ka; Nowaczyk et al., 2012) and between Greenland Interstadials (GIS) 9 and 8. The volumetrically large CI eruption was considered to have strongly affected the climatic system in the unstable climatic phase of the last glacial period that may even have triggered the strong cold period related to the marine H4 interval (40-39 cal kyr BP) and, as a result, human cultural changes and migration activities in this region (Fedele et al., 2002, 2008; Giaccio et al., 2008). This hypothesis, however, has been recently disproved by Lowe et al. (2012) who used the CI tephra to show that the onset of the H4 cold period predates the CI eruption. Therewith, the CI tephra forms an important stratigraphic marker in eastern Mediterranean palaeoclimatic and –environmental records that requires an unambiguous identification. These requirements are given in the Monticchio sequence, in which the CI is preceded and succeeded by a total of six other tephra layers of Campanian origin within a 2000 year period. One goal of our study is to clearly distinguish these six tephra deposits from the CI on the basis of their glass chemistry and mineral/lithic contents and to define distinct sources of them. A second goal is the investigation and interpretation of environmental impacts of the deposition of tephras of different thickness within the lake system and its catchment by applying high-resolution microfacies and µ-XRF elemental scanning techniques of tephra-hosting varved sediments. This information is crucial to help to detect and distinguish between primary and secondary (re-worked) tephra deposits and contribute to a better understanding of environmental and geomorphic responses following the deposition of tephras of differing thicknesses in the local catchment.

2. Regional setting

Lago Grande di Monticchio in Basilicata, southern Italy (40°56´N, 16°35´E), is the larger of two adjoining crater lakes that formed during the final stage of activities at 132 ± 12 ka

(Laurenzi et al., 1993; Brocchini et al., 1994), on the western slopes of the Monte Vúlture volcanic complex (Fig. 1). The lake surface of Lago Grande di Monticchio is situated at an altitude of 656 m a.s.l. and encompasses an area of ca. 0.4 km^2. The basin features a maximum depth of 36 m and a shallow water area with an average depth of 8.7 m in the southeast of the basin (Zolitschka and Negendank, 1996). The lake has a restricted hydrological catchment of 2.370.000 m^2 with a maximum elevation of 956 m a.s.l. (Zolitschka and Negendank, 1996). The trophic state of the present lake is eutrophic to hypertrophic promoting the preservation of annual laminations of its sedimentary deposits.

Situated approximately120 km east of Naples and in a favourable downwind position to high-explosive Campanian volcanoes, Lago Grande di Monticchio displays a unique trap for fallout tephras (e.g., Narcisi, 1996; Wulf et al., 2004, 2008, 2012). The Campanian volcanoes encompass several volcanic centres such as the Phlegrean Fields, the Somma-Vesuvius, as well as the islands of Ischia and Prócida-Vivara. Nearly all those centres are still active whereas the volcanic activity of the island of Prócida-Vivara ceded 14 cal ka ago with the deposition of the Torre Gaveta Tuff (Alessio et al., 1976). The Campanian volcanoes are petrologically classified as K-alkaline. The erupted products of the Phlegrean Fields and Procida-Vivara vary from a latitic to trachytic and alkali-trachytic to peralkaline phonolitic composition (e.g., D'Antonio et al., 1999; Pappalardo et al., 1999), whereas pyroclastics of Somma-Vesuvius are trachy-phonolitic to foiditic in composition (e.g., Santacroce et al., 2008). Eruptives from Ischia are mainly characterised by trachytes and alkali-trachytes of quite homogenous composition (Poli et al., 1989; Brown et al., 2008). During the time period of interest (ca. 40-38kyr) all four volcanic centres were explosively active and thus provide potential correlatives for tephras recorded in the Monticchio sediments.

3. Material and methods

3.1 Sample preparation

Seven macroscopically visible and primary tephra layers were analysed between 24.2 m and 27.4 m composite depth in the sediment record of Lago Grande di Monticchio (Fig. 2). These tephras are labelled according to Wulf et al. (2004, 2006) as TM-17-2, TM-18, TM-18-1a, TM-18-1b, TM-18-1c, TM-18-1d, and TM-18-2. Compositional studies including mineral-, lithic-, and glass assemblages, maximum grain-sizes and thicknesses of tephras (Table 1) as well as microfacies analyses of varved host sediments were carried out on large-scale thin sections (120 x 35 mm) from resin impregnated sediment slabs of cores LGM-B, -D, -L, -J and –M (Fig. 1; more core details are provided in Brauer et al., 2000, 2007; Wulf et al., 2004).

For geochemical analyses of tephras, polished thin sections (48 x 28 mm) of tephra bearing sediment slabs were produced ('in-situ-slides').

3.2 Glass geochemical analyses

At least 10 single glass shards of all seven tephras on the 'in-situ-slides' were analysed for their major and minor element composition using a CAMECA SX-100 probe with a 15 kV voltage, 20 nA probe current, a 15-20 µm beam diameter, and peak counting time of 20 s except for Na at 10 s. For the instrumental calibration, natural minerals and the glass reference standard "Lipari obsidian" was used (Hunt and Hill, 1996; Kühn et al., 2011). Prior to the EPMA measurements, glass shards were inspected under polarised light as well as by SE and BSE images in order to avoid hitting microcrystals that may cause accidental heterogeneity in glass compositions (e.g., Shane et al., 2008; Lowe, 2011). Single grain EPMA data of both the tephras and the glass reference standard are listed in Supplementary File 1. Mean values from EPMA are provided in Table 2 (non-normalised). All oxide values reported in the text and in Fig. 5 are normalised (water-free) data.

Tephras TM-18-1a, -b, -c and -d were additionally analysed for their trace elemental composition. Trace element analyses on individual glass shards were carried out using a Thermo Scientific iCAP Q ICM-MS coupled to a Photo Machines analyte 193 nm eximer laser ablation system with a Helix two volume cell at Trinity College Dublin. The fluence was 3.31 Jcm^{-1}, and we used a 24 µm spot, a repetition rate of 5 Hz, and a count time of 40 seconds (200 pulses). Concentrations were calibrated using NIST612 with ^{29}Si as the internal standard. Data reduction was performed manually using Microsoft Excel following the method of Tomlinson et al. (2010). Analyses of MPI-DING glass StHs6/80-G typically gives accuracies of <5%. Reproducibility of StHs6/80-G analyses is <5 RSD% for all trace elements except Er, Th and U which are <10% RSD and close to detection limit. Relative standard errors are typically 1-5% for most elements and <7% for Sr, Ba, Eu. Full errors (standard deviations and standard errors for individual sample analyses) are given in Supplementary File 1. Trace element data of samples TM-18-1a, -b, -c and -d were compared with published data from tephra TM-18 (Tomlinson et al., 2012).

3.3 The µ-XRF elemental scanning and microfacies analysis

To identify primary and reworked tephra material and to detect potential environmental changes after tephra deposition, a combination of µ-XRF elemental scanning and microfacies analyses on the 3.2 m long sequence of tephra-hosting sediments was applied.

The µ-XRF core scanning was carried out on cleaned, smooth surfaces of five sediment cores LGM-O9-u (60-92 cm), LGM-O10-o (0-100 cm), LGM-O10-u (0-97 cm), LGM-M12-o (54.5-97 cm), and LGM-M12-u (0-23 cm). Except for tephras TM-18-1b and TM-18-2, all tephras studied occur in these cores. µ-XRF measurements were carried out on an ITRAX core scanner (COX Analytical Systems, Sweden) operated with a molybdenum (Mo) tube, an accelerating voltage of 30 kV, and a beam current of 30 mA. The step size of measurements was 200 µm and the exposure time 20 s per measurement. In order to detect relative changes in the elemental composition of sediments and tephra deposits, major and minor elements with significant variations (such as Si, K, Ca, Ti and Mn) were chosen for interpretation (Fig. 2; Supplementary File 2).

The µ-XRF core scanning was supported by microfacies analysis that encompassed the microscopic description and classification in "lithozones" of the tephra-hosting sediments using overlapping large-scale thin sections of the B/D-, L-, J- and M- core. Microscopic description was carried out using a Zeiss-Axioplan- and a Zeiss-Axiophot microscope with a 50-400-times magnification. For detection of sedimentological changes the focus of microfacies analysis was set on the tephra layers and immediately under- and overlying sediments.

3.4 Chronology

Tephra ages were obtained from the varve supported sedimentation rate-derived chronology of the Monticchio sequence, which was initially established by Zolitschka and Negendank (1996) and Brandt et al. (1999) and updated by Brauer et al. (2007). Annual laminations in the section of interest are very well preserved. Tephra TM-18 (CI) was additionally dated by $^{40}Ar/^{39}Ar$ analysis of sanidine at 37 ± 3 ka and 35 ± 1 ka (Watts et al., 1996; Wulf et al., 2004). The varve and radioisotopic ages of TM-18 appear approximately 2500 years too young in comparison to the well-accepted $^{40}Ar/^{39}Ar$ age of 39.28 ± 0.11 ka of proximal CI deposits (De Vivo et al., 2001), indicating an underestimation of varve counts of approximately 6 % in the preceding and/or succeeding poorly varved sections (Wulf et al., 2012). However, varve ages of the remaining tephras in the Monticchio sequence can still be used for differential dating by calculating the time of deposition relative to the eruption of the Campanian Ignimbrite (Table 1).

4. Results and Discussion

4.1 Sediment composition

The sediments in the studied sections are predominately annually laminated, and varves are comprised of different contents of autochthonous (i.e., calcite precipitates, siderite, pyrite, vivianite, diatoms) and allochthonous components (i.e., epiclastic material of older Mt. Vulture volcanics, terrestrial plant remains from the catchment, benthic diatoms). Biochemical calcite precipitation occurs in early summer, when pH values and temperatures of the lake water increase (Zolitschka, 1990) (Figs. 3C, D). Siderite often also forms layers immediately after the precipitation of calcite (late summer-autumn), whereas early diagenetic pyrite is irregularly scattered throughout the interval of interest. Vivianite is rare and occurs exclusively in the lower part of the sediment section (Fig. 4C). The latter components indicate an anoxic environment with a high availability of Fe^{2+} ions as well as carbonate (siderite), sulphate (pyrite), and phosphate (vivianite) concentrations (Zolitschka, 1990; Matthes, 1999). Diatoms are abundant and occur as spring and autumn layers in the sediments. Predominately planktonic species were found, i.e. mainly *Stephanodiscus spp.*, *Cyclotella spp.*, and subordinately *Fragilaria spp.* and *Crysophyceae* cysts in the upper sediment section (Fig. 3D, 4C). Allochthonous material is mainly found within detrital layers (turbidites and slump deposits) transported from the catchment and the littoral zone into the lake basin from erosional processes. Tephra material is also an allochthonous component, which is either directly deposited by fallout from an eruption cloud or re-deposited in turbidites and slumps because of catchment erosion.

4.1.1 Lithology

Based on detailed microfacies analyses the sediments in the section of interest can be divided into four lithologies, L1 to L4:

- L1 is characterised by homogenous organo-clastic sediments with a mixture of primary planktonic diatoms and to a lesser extend minerals and plant remains.
- L2 consists of laminated sediments with a very high amount of planktonic diatoms (*Cyclotella spp.*, *Stephanodiscus spp.*). The lamination is made up of alternating sub-layers of autochthonous calcite, siderite, and diatoms (here defined as "Type A varves"). Calcite layers do not occur on a regularly basis with the result that some sections are solely dominated by alternating siderite and planktonic diatom layers. Some sections are even reduced in diatoms and enriched in detrital layers. In such intervals siderite and calcite are absent. A common feature of L2 is the infrequent occurrence of vivianite (Fig. 4C).

- L3 is characterised by turbidites, which are suspension flows with a coarser grained base, mostly consisting of epiclastic components, and a gradually decrease in grain size towards the top (dense clay layer).
- L4 is characterised by laminated sediments. The main difference from L2 is the abundance of diatom species of *Fragilaria spp.* together with *Crysophyceae.* Laminations encompass autochthonous calcite layers, underlain by diatom layers made up of *Fragiliaria spp.*, and an organo-clastic layer (here defined as "Type B varves") (Figs. 3C, D). The definitive properties of the sediments enclosing the tephra layers can be seen in Table 3.

The four lithologies alternate within the sediments under study (Fig. 2). The topmost part above tephra TM-17-2 is characterised by well-laminated sediments of L4, whereas sediments between tephras TM-17-2 and TM-18 (CI) are dominated by homogeneous L1 deposits, L3 turbidites and minor well-laminated L2 sections. L2 varves below TM-18, in turn, are well preserved and sporadically alternate with homogeneous L1 sediments and minor L3 turbidites above and below tephra TM-18-1c, respectively (Fig. 2). All tephras investigated are enclosed in a sediment matrix that is characterized by exceptional varve preservation.

4.1.2 µ-XRF elemental profiles

µ-XRF element data are characterised by relatively low variations of the elements silicon (Si), titanium (Ti), calcium (Ca), potassium (K), and manganese (Mn) with some exceptional peaks attributed to special layers (Fig. 2, Supplementary File 2). Ti-peaks, for example, can be attributed to Fe-Ti oxides (e.g., titanomagnetite) in epiclastic material (volcanoclastic deposits derived from the catchment) in turbidites, which most likely was washed from the catchment into the lake and are often found in L2 and L3 above tephra TM-18. Mn peaks occur in L2 and are found in the sediment sections underneath TM-18-1c and TM-18-1d. Ca peaks are related to authochthonous calcite layers and also occur within tephra TM-17-2, where detrital carbonates form a major component. Except for TM-18-1b and TM-18-2 not represented in the cores analysed, all other tephra layers reveal elevated K counts in comparison with those of the enclosing sediments. Some tephras are partially enriched in other elements such as Mn (TM-18-1c, TM-18-1-d), Ca (TM-17-2, TM-18-1d), and Si (TM-17-2, TM-18-1a, TM-18-1c, TM-18-1d). Reworked tephra layers identified by thin section microscopy can also be traced by distinct K peaks (Fig. 2, Supplementary File 2), though quantities are smaller in these layers compared with the amounts in the primary tephra deposit, because the signals primarily from the glass shards are diluted with other sediment components.

4.2 Composition and origin of tephras

The results of compositional and geochemical analyses (normalised data) of the seven distinct tephra layers in the Monticchio record, from youngest to oldest, are presented in detail (Tables 1 and 2). Tephra ages are given as calendar ages with a mean 5% counting error (Wulf et al., 2012). Overall, geochemical glass data of all tephras reveal a similar K-alkaline composition indicating a provenance from Campanian volcanoes in Southern Italy.

4.2.1 Tephra TM-17-2 is a 2-cm thick, brown layer at 24.30 m composite depth (Figs. 3A, B) and is dated at 35,530 ± 1780 varve yrs BP. The mineral assemblage comprises phenocrysts of sanidine, clinopyroxene, biotite, plagioclase, amphibole, and Fe-Ti oxides. In the lithic assemblage, detrital carbonates are dominant (Fig. 3B), whereas volcanic rock fragments are rare. Volcanic glass shards are brown or colourless, often platy or cuspate shaped and rich in apatite and clinopyroxene microcrystals. Probably because of the high amount of microcrystals, glass shards show a heterogeneous trachytic glass composition with the highest and most variable concentrations in SiO_2 (62.3-67.5 wt%), CaO (2.0-3.9 wt%), and alkali ratios (K_2O/Na_2O) of 1.8-2.8 (Table 2). The glass major and minor element compositions, the mineral assemblage, the lithic content of volcanic rock fragments and distinctive detrital carbonates, and the age point to an origin of tephra TM-17-2 from the Schiava eruption of Somma-Vesuvius. This eruption reflects most likely the oldest activity at Somma-Vesuvius (Di Vito et al., 2008) occurring between the eruption of the Campanian Ignimbrite (Phlegrean Fields, 39.3 ka; De Vivo et al., 2001) and the Pomici di Base eruption (Somma-Vesuvius, ca. 22 cal ka BP; Santacroce et al., 2008). Di Vito et al. (2008) described the "Schiava Pumices" that in medial-distal locations northeast of Vesuvius are deposited on a thin palaeosol at the top of the Campanian Ignimbrite (Di Vito et al., 2008). They are characterised by white alternating ash and lapilli beds with highly vesicular pumice (Di Vito et al., 2008) showing a similar trachytic composition as tephra TM-17-2 with increased SiO_2 concentrations accompanied by low alkali and low FeO_2, TiO_2, Al_2O_3, and MgO values (Fig. 5, Table 2). The Schiava pumices are furthermore correlated with the marine tephra C-9 in Tyrrhenian Sea core KET 8004 and KET 8011, where it is dated by oxygen isotopes at ca. 36 ka (Paterne et al., 1988; Paterne and Guichard, 1993).

4.2.2 Tephra TM-18 has been previously correlated with the Campanian Ignimbrite (CI) from the Phlegrean Fields (Narcisi, 1996; Wulf et al., 2004) and is dated in the Monticchio record

at 36,770 ± 1840 varve yrs BP (Wulf et al., 2012). The thicknesses of TM-18 show large variations between cores: 17.2 cm (core LGM-B/D), 20.5 cm (core LGM-L), 26.5 cm (core LGM-M), and up to 35.5 cm (core LGM-O). TM-18 is best preserved in core LGM-J where it occurs as a 23-cm thick greyish-beige layer that can be divided into a basal coarse grained pumice fall layer and an overlying co-ignimbritic fallout layer of equal thickness (Fig. 6A). Those have been assigned to the proximal CI fall and flow (lower, intermediate, and upper), respectively (Tomlinson et al., 2012) (Fig. 2). The basal pumice fall layer is further divided into two main units: a 12.5 cm thick lower pumice fall layer and a 4.1 cm thick upper pumice fall layer (Fig. 2). These units and sub-units are directly comparable with the proximal stratigraphy of the CI fall unit after Rosi et al. (1999), and therefore we use the same code names in our description. The lower pumice fall layer in Monticchio, corresponding to the Lower Fall Unit "LFU" after Rosi et al. (1999), is light grey to grey in colour and consists of coarse grained, inversely and ungraded pumice deposits. In general, micro-pumices are whitish to light grey and are highly to extremely vesicular, showing round and tubular vesicles (Figs. 6B1, B2). They are accompanied by cuspate shaped, colourless and brown glass shards. The lithic assemblage is mainly made up of volcanic rock fragments, whereas the mineral assemblage comprises clinopyroxene, plagioclase and sanidine phenocrystals. The lower pumice fall layer is further divided in three sub-layers V1 to V3 based on additional components to the basic composition described above. In the lowermost sub-layer V1, Fe-Ti oxides additionally occur, whereas in the middle sub-layer V2 biotite is found for the first time. The uppermost sub-layer V3 is characterised by pumices with black iron microcrysts and maximum grain sizes of 8 mm, and is accompanied by amphiboles in the mineral assemblage. The upper pumice fall layer in Monticchio, corresponding to the Upper Fall Unit "UFU" after Rosi et al. (1999), is greyish-beige in colour, ungraded and comprises pumice clasts with an increased amount of lithics and loose minerals as well as bi-coloured glass shards (Fig. 6B3). The composition of the lithic and mineral assemblage of UFU is similar to that of the LFU. UFU is further sub-divided in four sub-layers: In the lowermost sub-layer V4, a high amount of biotite and an increased amount of glass shard are found. Besides volcanic rock fragments, sedimentary rock fragments are found in the succeeding sub-layer V5. Sub-layer V6 is coarser grained, with a high amount of lithics and pumice clasts whereas the uppermost sub-layer V7 contains a crystal-rich ash layer comprised of accumulated brown glass shards with subordinated lithics and an increased amount of loose crystals. The coarse basal fallout deposits (LFU, UFU) in Monticchio are directly overlain by a finer grained co-ignimbrite layer mainly comprised of cuspate shaped, colourless and brown glass shards. This

fall layer can be related to the second phase of the CI eruption characterised by a caldera collapse and the eruption of three pyroclastic density currents (e.g., Ort et al., 2003), which Tomlinson et al. (2012) refer to as lower, intermediate, and upper ignimbritic flow units, respectively.

Geochemical analyses of pumices and glass shards throughout the entire TM-18 deposit reveal a rather homogenous phonolitic-trachytic composition with concentrations in SiO_2 of 61.1-62.9 wt%, CaO of 1.6–2.0 wt%, and alkali ratios of 0.9 to 1.4 (Fig. 5, Table 2). Only one single glass shard shows a K-trachytic composition with a lower SiO_2 value (60.1 wt%), higher CaO concentration (2.31 wt%), and an alkali ratio of 1.8 (Table 2). According to Tomlinson et al. (2012), the main glass population of TM-18 is typical for that of both proximal fall units LFU and UFU and the lower and intermediate ignimbritic flow units of the CI, whereas the minor glass phase is representative for the upper ignimbritic flow unit. These geochemical variations are also reflected in the trace element composition of TM-18 (Tomlinson et al., 2012). The main glass population from the fall units and the lower and intermediate flows is compositionally intermediate to evolved with Zr/Sr ratios of 15-35, whereas the juvenile phase from the upper flow is less evolved with Zr/Sr ratio of 0.3 (Tomlinson et al., 2012). The fall and flow units of TM-18 can be best distinguished on the basis of some HFSE incompatible elements such as Th, U, Zr and Nb, which are typically higher in the fall and lower/intermediate flow units (Th, 41-53 ppm; U, 15-19 ppm; Zr, 549-667 ppm; Nb, 99-120 ppm; U/Nb ratios of 0.14-0.16; Zr/Nb ratios of 5.0-5.6) than in the upper flow unit (Th, 15 ppm; U, 5 ppm; Zr, 185 ppm; Nb, 31 ppm; U/Nb ratio of 0.16; Zr/Nb ratio of 6.0) (Tomlinson et al., 2012) (Fig. 8).

4.2.3 Tephra TM-18-1a is a 3.2-cm thick inverse-graded, greyish-beige, vitric tephra located in a composite depth of 26.59 m, ca. 11 cm below the CI deposit (Fig. 7A). It is dated by the Monticchio chronology at 36,840 ± 1840 varve yrs BP, and therewith deposited approximately 70 varve yrs before the TM-18/CI tephra. The loose mineral assemblage consists of sanidine, subordinated plagioclase, clinopyroxene, and biotite, whereas lithics comprise volcanic rock fragments. The fine-grained glass matrix is mainly made up of cuspate colourless glass shards, whereas brown glass shards are subordinate and rich in apatite microcrystal inclusions (Fig. 7B). Pumice fragments and glass shards are highly vesicular and show a homogenous phonolitic-trachytic composition that is very similar to that of TM-18 (61.1-62.2 wt% SiO_2; 1.7-2.0 wt% CaO; alkali ratios of 1.2-1.3) (Fig. 5, Table 2). Trace element contents of TM-18-1a glasses weakly match the TM-18 fall and

lower/intermediate flow units in terms of slightly higher concentrations in Nb (106-133 ppm) and Zr (601-937 ppm) and lower values in Th (15-40 ppm) and U (5-10 ppm) resulting in higher U/Nb (0.15-0.19) and Zr/Nb (5.3-7.2) ratios (Fig. 8). The composition of TM-18-1a suggests a similar origin as the CI from the Phlegrean Fields.

4.2.4 Tephra TM-18-1b is a fine-grained, 6-mm thick vitric tephra located in 26.66 m composite depth (Fig 7A). It was deposited at 36,940 ± 1850 varve yrs BP, approximately 170 varve yrs prior to the deposition of TM-18/CI tephra. It shows weak normal grading and encompasses phenocrysts of sanidine, biotite, plagioclase, and minor clinopyroxene. Lithics are equally spread in the tephra and consist of volcanic rock fragments. Juvenile clasts comprise white and brown glass shards, whereas brown glass shards are more frequent and rich in apatite microcrystals (Fig. 7C). TM-18-1b shows a homogenous phonolitic-trachytic glass composition with concentrations in SiO_2 at 60.7-61.7 wt%, CaO at 1.7-1.9 wt%, and alkali ratios of 1.2-1.4 (Table 2). Both the major and trace element glass compositional data of TM-18-1b overlap with those of TM-18 except that it has slightly higher concentrations of incompatible elements (e.g. Zr, 537-738 ppm) (Figs. 5, 8). The glass composition of TM-18-1b implies a possible source from the Phlegrean Fields.

4.2.5 Tephra TM-18-1c is a 5-mm thick, inverse graded, white-beige, vitric ash in 26.75 m composite depth (Fig. 9A). TM-18-1c is dated at 37,060 ± 1850 varve yrs BP and is approximately 290 varve yrs older than the TM-18/CI tephra. It mainly comprises highly vesicular, colourless glass shards with tubular vesicles (Fig. 9B). Crystals are rare and include sanidine, plagioclase, and minor clinopyroxene phenocrystals. Volcanic rock fragments are subordinate and occur scattered in the tephra layer. In addition, secondary pyrite occurs at the base of TM-18-1c. Glass major element data display a homogenous phonolitic-trachytic composition with contents in SiO_2 of 61.3-61.8 wt%, CaO of 1.7-1.8 wt% and alkali ratios of ~1.2 resembling that of the succeeding tephras from the Phlegrean Fields (Fig. 5, Table 2). Trace element data are the least distinctive overlapping with TM-18-1a and TM-18-1b at low trace element contents (e.g., Zr, 600-983 ppm; U, 18-23 ppm), but differing from the CI with slightly higher values in Th (47-84 ppm) and Nb (110-150 ppm) (Fig. 8).

4.2.6. Tephra TM-18-1d occurs in a sediment depth of 27.04 m, dates at 37,360 ± 1870 varve yr BP and thus is 590 varve yrs older than TM-18/CI. It is a 1-cm thick, grey to brownish tephra layer with a normal gradation and a bimodal glass composition (Figs. 9C, D). Pumice

fragments and glass shards are bubble-wall or cuspate shaped, low to highly vesicular and show inclusions of apatite microcrystals to some extent. The mineral assemblage comprises sanidine, clinopyroxene, subordinately plagioclase, and biotite. The lithic assemblage includes fragments of volcanic rocks. Glass shards are also phonolitic-trachytic but bimodal in composition with alkali ratios of 1.1 (majority of data) and 2.1 (one data point) and slightly decreased SiO_2 concentrations of 59.7-61.2 wt% compared to those of glass from TM-18, TM-18-1a, TM-18-1b, and TM-18-1c (Table 2, Fig. 5). The trace element composition of TM-18-1d forms a distinct field at the highest incompatible element contents (Th, 53-89 ppm; U, 21-33 ppm; Nb, 131-198 ppm; Zr, 681-1072 ppm) (Fig. 8). Based on its glass composition we propose an origin of this tephra from the Phlegrean Fields.

At this point, a detailed correlation of tephras TM-18-1a, TM-18-1b, TM-18-1c, and TM-18-1d with dated explosive proximal events is rather difficult because of the similarity of the major and trace element composition of glasses of these tephras and the lack of single grain EPMA glass data of proximal tephra deposits for comparison. Furthermore, these tephras (TM-18-1a to -d) are deposited within a time interval of ca 600 varve yrs prior to the TM-18/Campanian Ignimbrite eruption requiring clear chronostratigraphic constraints and high-resolution dating techniques that are not yet available for proximal deposits. However, some potential correlatives are provided from the proximal Torregaveta (TG) and Trefola (TL) sections in the west and north of the CI caldera, respectively (Pappalardo et al., 1999). In the Trefola section, the Campanian Ignimbrite is underlain by 11 pyroclastic units, of which the youngest one TLm has been $^{40}Ar/^{39}Ar$ dated at 45.6 ± 0.7 ka (Pappalardo et al., 1999). The TG section documents a sequence of 12 pyroclastic fall and flow deposits separated by palaeosols underneath the CI deposits, each palaeosoil representing a hiatus. The uppermost three units from top to base, TGm (flow), TGl, and TGk (fallout), are related to activity in the Phlegrean Fields and are underlain by Ischia tephra layer TGj (Pappalardo et al., 1999). The three tephras from the Phlegrean Fields all closely match the major and trace element chemical compositions of glasses from both the CI and tephras TM-18-1a to TM-18-1d (Figs. 5, 8). A study from the medial-distal terrestrial sites on the Sorrentina Peninsula (SMP1/SMP2) and near Cervino (CE1), located approximately 30 km southeast and northeast of the Campanian Ignimbrite caldera, respectively, reveals three trachyphonolitic fallout deposits between the CI and the Santa Lucia tephra (ca. 51 ka; Sulpizio et al., 2003; Di Vito et al., 2008). The lowermost of these pyroclastic deposits, CE1-d, does not fully match the major element glass composition of the Monticchio tephras, but approximates that of one single

glass shard of tephra TM-18-1d (Fig. 5). The stratigraphically younger medial-distal pyroclastic unit, SMP1-a, has been tentatively linked to Ischia eruptives (Di Vito et al., 2008) and is correlated with marine distal tephras C-14 (41.8 ka; Paterne et al., 1988; Sulpizio et al., 2003) and PRAD1752 (Bourne et al., 2010) from the Tyrrhenian (core KET80-04) and Adriatic Seas (core PRAD1-2). Bourne et al. (2010) suggested a rough correlation of PRAD1752 with one of the Monticchio TM-18-1 layers. Damaschke et al. (2013), in turn, suggested a more specific allocation and assigned cryptotephra PT0915-8 (ca 44 ka) in Lake Prespa (Balkans) to both SMP1-a and Monticchio tephra layer TM-18-1d. The major element glass composition of SMP1-a (Sulpizio et al., 2010) indeed shows the best chemical match with the main glass population of TM-18-1d, while the Prespa and PRAD tephras also overlap with the other TM-18-1 tephras (Fig. 5). The comparison of trace element data of SMP1-a (bulk data) with the Monticchio tephras (single grain data), however, does not provide any clear correlation (Fig. 8B). The uppermost medial-distal tephra SMP1-c, directly underlying the CI deposit, has been correlated with the marine tephra C-13b (Paterne et al., 1988; Sulpizio et al., 2003). SMP1-c does not match any of the Monticchio tephras, but approximates the glass chemistry of one single shard of TM-18-1d (Fig. 5). In conclusion, the proposed correlations suggested here are tentative and require further testing via additional EPMA-WDS and single grain trace element data.

4.2.7 Tephra TM-18-2 is a 1-mm thick, normally graded, white vitric ash (Figs. 4A, B) that is found in a composite sediment depth of 27.22 m and dates at 37,580 ± 1880 varve yrs BP. It predominately comprises pumice clasts, which are whitish to grey and highly to extremely vesicular with round vesicles (Fig. 4B). Glass shards are bubble-wall and cuspate shaped and exhibit inclusions of apatite needles to some extent. The phenocryst content is made up of sanidine and plagioclase, whereas biotite and clinopyroxene are rare. Lithics are scattered volcanic rock fragments which to some extend reveal adherent glass. The glass chemical data reflect a homogenous trachytic composition characterized by increased SiO_2 values (63.6-64.7 wt%), low CaO values (~ 1.4 wt%) and alkali ratios (1.1-1.4) (Fig. 5, Table 2). The glass composition of TM-18-2 slightly differs from that of the TM-18-1 tephras, indicating an origin from the Island of Ischia rather than from the Phlegrean Fields. The 44-33 ka period saw the deposition of a series of pyroclastic products, collectively termed the Citara Formation (Poli et al., 1987), one of which may be a potential correlative for TM-18-2 (Fig. 5). The Citara Formation is tentatively linked to Ischia layer TGj from the proximal/medial-distal Torregaveta site (Pappalardo et al., 1999), but the marine C-14 tephra dated at 41.8 ka

BP in Tyrrhenian and Adriatic Sea cores (Paterne et al., 1988) so far provides the best geochemical match (Fig. 5).

4.3 Environmental and ecological responses of tephra deposition

We focus on the reworking processes of individual tephra deposits, from oldest to youngest, in the Monticchio record. Based on a combination of µ-XRF scanning and thin section microscopy different amounts of reworked tephra material and changes in the sedimentation rates were detected directly after the deposition of primary tephra fallout deposits. A detailed overview of µ-XRF elemental data of reworked sections is provided in Supplementary File 2.

4.3.1 Tephra TM-18-2

Tephra TM-18-2 is enclosed within weakly laminated L2 sediments consisting of alternating layers of planktonic diatoms (summer layers of *Stephanodiscus* and *Cyclotella*) and organo-clastic reworked material (winter layers made up of epiphytic diatoms and organic matter from the littoral zone and the shore) (Fig. 4A, C). Planktonic diatom layers are dark grey in colour and range from 70 to 100 µm in thickness below the tephra deposit, whereas the reworked layers are lighter in colour, thinner (20 to 50 µm), and sometimes include scattered blue vivianite crystals in addition to pyrite and fine calcite crystals (Fig. 4C). Sediments above tephra TM-18-2 are well varved showing a similar structure but increased thicknesses of ca. 100 µm for each the summer and winter sub-layer. Reworked tephra material (glass shards) is accumulated in the detrital winter layer especially in the first year after tephra deposition whereas in the following five years only scattered reworked glass shards occur.

4.3.2 Tephra TM-18-1d

Tephra TM-18-1d is underlain by well varved L2 sediments characterised by alternating planktonic diatom (ca. 100-µm thick summer layers) and detrital and reworked layers (ca. 50-µm thin winter layers made up of benthic diatoms, plant remains, epiclastic material). Following the deposition of tephra TM-18-1d, four distinct reworked tephra layers with a total thickness of 1 cm occur (Fig. 9C; Supplementary File 2e). The first reworked tephra layer is characterised by fine-grained glassy material and complemented by extremely fine-grained clayey material at the top (normally graded). The second reworked layer shows a fine-grained glassy matrix of glass shards (bimodal), subordinate lithics and minerals with interspersed planktonic diatoms whereas the third layer is comprised of coarser grained minerals, lithics, and glass shards as well as benthic diatoms and plant remains. The fourth reworked layer

mainly comprises colourless and brown glass shards scattered in planktonic and subordinate epiphytic diatom species. The first and second reworked layers are attributed to intra-lake reworking, while the third and fourth reworked layers most likely represent run-off from the catchment. The reworked tephra layers are overlain by a section of laminated sediments (62 varve years) that are characterised by alternating layers of planktonic diatoms (summer layer) and detrital/reworked layers (winter layer) that contain gradually decreasing amounts of reworked tephra material. Higher concentrations of reworked glass shards and an increase in thickness of planktonic diatom and detrital layers is found in the varves up to ten years after the primary tephra deposition. Forty-eight varve years after TM-18-1d was deposited, higher concentrations of reworked tephra material occur in a distinct coarse-grained turbidite and in the detrital layers of the following two years.

4.3.3 Tephra TM-18-1c

The L2 sediments underlying TM-18-1c show a weak lamination with alternating layers of planktonic diatoms (thickness 100 µm) and thin detrital and reworked layers (50 µm) made up of abundant plant material from the catchment and benthic diatoms from the littoral zone, respectively (Fig. 9A). In addition, calcite, siderite, vivianite, and pyrite occur scattered in these layers. The overlaying sediments show an indistinct lamination with the same alternating sequence and composition as the underlying sediments, excluding vivianite. In the second and third years after tephra deposition, thickness of both planktonic diatom layers (thickness 200 µm) and detrital/reworked layers (100 µm) increased. Reworked glass shards of TM-18-1c is found up to 30 years after the primary deposited tephra TM-18-1c and occur scattered in detrital and reworked layers as well as in the bases of three turbidites occurring 1.5 cm, 2.6 cm, and 3.8 cm above the tephra (Fig. 9A; Supplementary File 2d).

4.3.4 Tephra TM-18-1b

Tephra TM-18-1b is encapsulated in homogenous L1 matrix sediments consisting of planktonic diatoms, siderite, pyrite, plant remains, and interspersed benthic diatoms (Fig. 7A). The boundaries of this tephra with respect to the surrounding sediments are not as sharp as for the other primary tephra layers. Reworked tephra material is detected beneath and above the primary tephra layer. The section underneath the tephra is characterised by the occurrence of pumices and glass shards lenses that penetrate into the sediments up to 5 mm, suggesting bioturbation processes. In the overlaying sediments scattered reworked tephra material (glass shards) occurs up to 2 cm above the ash layer showing a gradually decrease of glass shard

concentration. An increase of the planktonic diatom population after the primary tephra deposition was not observed.

4.3.5 Tephra TM-18-1a

Tephra TM-18-1a is encased within L1 and L2 sediments which are faintly varved to massive (Fig. 7A). The sediment is mainly composed of planktonic diatoms (*Cyclotella spp., Stephanodiscus spp.*) and subordinate loose epiclastic material. Plant remains occur in very high amounts accompanied by siderite especially immediately underneath the tephra layer. In general, siderite and pyrite occur uniformly in the sediment. In the sediments underneath the tephra, lenses and filled burrows of pumice appear, indicating bioturbation processes. Tephra layer TM-18-1a is directly overlain by three reworked tephra layers with a total thickness of 2.5 cm (Fig. 7A; Supplementary File 2c). The first reworked layer is 5 mm thick and comprises a mixture of fine-grained (<100 µm), reworked tephra material (glass shards, pumices, lithic fragments, and loose mineral grains) and planktonic diatoms. Its formation can be most likely ascribed to intra-lake reworking processes. The second reworked layer is 3 mm thick and is dark, greenish to black in colour. It mainly consists of coarser grained (ca. 200 µm) epiclastic material from the lake catchment encompassing a high amount of lithics and minerals (green clinopyroxene, biotite, amphibole, sanidine, plagioclase) at the base and subordinate pumice fragments, benthic diatoms and plant remains in the upper part of the layer. This reworked layer most likely resulted from catchment erosion and re-depositional processes from the littoral zone. The third reworked tephra layer is 1.7 cm thick and shows a fine-grained glassy matrix interspersed with a very high amount of planktonic diatoms and a lower amount of benthic diatoms, plant remains, siderite and epiclastic minerals. It is noticeable that the glassy matrix is vertically crossed by burrows (bioturbation). Inside the burrows scattered reworked tephra material occurs. After the deposition of the distinct reworked tephra layers a gradually decrease of glass shards is determined in the varved sediments and only scattered glass shards are found ca 5 cm up to the next tephra layer TM-18 (Supplementary File 2c).

4.3.6 Tephra TM-18

The Campanian Ignimbrite is underlain by faintly laminated L2 sediments which are split by thick siderite layers with a maximum thickness of 0.5 mm (Figs. 6A, 7A). The siderite layers alternate with mixed layers of planktonic and benthic diatoms, whereas the sediment directly underlying the tephra shows a more massive appearance with very weak lamination. This

section mainly comprises planktonic and benthic diatoms with scattered minerals and plant remains. In addition, pyrite is homogenously distributed, whereas siderite is very sparse. The sediments overlying the tephra layer are weakly laminated (L2 and L3 type sediments) and are characterised by reworked tephra material and planktonic diatoms layers. Reworked glass shards have been found up to 186 cm above the primary deposited tephra. The reworked CI deposits can be subdivided into three sections (Fig. 6; Supplementary Files 2a, b, and c). The first section immediately above the primary CI tephra is 1.7 cm thick and comprises eight varve years. Varves are made up of alternating reworked tephra layers (mixtures of glass shards, lithics, loose crystals, and a high amount of planktonic diatoms) and planktonic diatom layers. Within this section, the third year after tephra deposition shows a particular increase in diatom abundance and a change in size of planktonic species, which is followed by distinct planktonic diatoms layers (average thickness of 150 µm) in the eighth varve after the tephra fall. Because of the high amount of glass shards in this section, K-values obtained by µ-XRF core scanning are indistinguishable from those obtained on the primary CI deposit. Re-deposition of tephra material in the first section can be most likely attributed to intra-lake reworking processes. The second section of reworked tephra is 1.5 cm thick and is characterised by a weak lamination of alternating layers of mixed coarser-grained organic material and tephra (pumices, bimodal glass shards, minerals, lithics) and distinct planktonic diatoms layers. Here, reworked tephra layers are more distinct from the sediment matrix forming individual K-peaks via the µ-XRF scans. The presence of epiphytic diatoms and terrestrial plant remains within the reworked tephra layers point to erosional in-washing processes from the shore/catchment. The third section of reworked tephra material is characterised by an array of turbidites. In total, 15 normal graded turbidites with reworked TM-18 tephra material (glass shards and pumices) at the base and overlying finer-grained epiclastic material from the catchment (i.e., altered pumices, minerals and lithics of older Mt. Vulture pyroclastic deposits) occur. The amount of tephra derived glass shards decreases towards the top of this section, but scattered reworked TM-18-derived glass shards are present in the sediments right up to the next primary tephra (TM-17-2), i.e. spanning over a period of 1240 varve years.

4.3.7 Tephra TM-17-2

The sediments encapsulating TM-17-2 are well laminated (L4 sediments) and the varves are characterised by an alternation of autochthonous calcite and organogenic sub-layers (Figs. 3A, C, D). The section underlying the tephra can be sub-divided into two sub-sections showing a

fine laminated section and a thicker laminated section which is located immediately beneath the tephra (Fig. 3A). The fine laminated section shows varves with an average thickness of 0.8 mm. They comprise a thin layer of diatoms with elongated planktonic *Fragilaria spp.* which are typical for mesotrophic- to oligotrophic water bodies, and other planktonic species, followed by a layer of calcite and a layer of organoclastic material (Fig. 3D). Siderite is rare, whereas pyrite is commonly dispersed in the clastic material. However, the thicker laminated section is characterised by varves with an average thickness of 2.1 mm. They are composed of a thin diatom layer followed by a calcite layer and a layer primarily made up of siderite. The increase in siderite starts six varves before tephra TM-17-2 was deposited and is accompanied by an increase of clastic material. Especially in the two varves preceding the tephra fall, coarse-grained loose minerals of epiclastic material derived from the catchment are present. Here, pyrite also occurs within calcite layers. The sediments overlying the tephra are laminated but show "disturbed" sections especially in the first four years after tephra deposition (Fig. 3A). These disturbed sections are characterised by a mixture of loose calcite crystals in addition to planktonic diatoms (*Stephanodiscus, Cyclotella*), *Chrysophyceae,* and reworked tephra in the form of glass shards with microcrystal inclusions and phenocrysts indicating intra-lake reworking processes. Scattered glass shards of TM-17-2 are found up to 10 years after the primary tephra deposit, which is also confirmed by slightly elevated K-counts of sediments (Supplementary File 2a). Thicker planktonic diatom layers of *Stephanodiscus* and *Cyclotella* occur in the second and third year after the primary tephra layer. The reworked section again is followed by a finer laminated section similar to that of the underlying sediment section with *Chrysophyceae* interspersed in the *Fragilaria* layer.

5 Syntheses

5.1 Detection of tephras, their reworking and environmental impact of tephra deposition

Reworked tephra material (mainly volcanic glass shards) is commonly found in the sediments overlying the primary tephra layers. The detection of this tephra material is possible by combined microscopic thin section studies and µ-XRF elemental scanning. The sensitivity of the latter strongly depends on the concentration of glass shards and the composition of host sediments (e.g., Kylander et al., 2011; Damaschke et al., 2013; Wulf et al., 2013). Tephra material of phonolitic-trachytic composition is clearly traceable by increased counts in potassium (Fig. 2, Table 3). Tephra layers TM-18-1c and TM-18-1d even show increased counts in manganese providing a useful signal for detecting their reworking. TM-17-2 which is intercalated in a rather calcareous sediment matrix compared with that of the other six

tephras is additionally characterised by increased counts in silica (Fig. 2, Table 3). Reworked tephra material shows also increased K counts, but the intensity of K counts strongly depends on the concentration of glass shards in the primary tephra layer.

The processes for reworking of tephra material are a combination of intra-lake processes, especially movement from the littoral zone, and external processes that include detrital influx/runoff from the catchment. Intra-basin reworking processes are reflected by a mix of tephra-derived glass shards and planktonic or epiphytic diatoms, or both, and the lack of detrital catchment-derived material. These processes occur immediately after the ash fall and last up to 8 years (e.g., TM-18/CI) after the primary tephra deposition. The products of runoff processes from the catchment are superimposed on the materials reworked by intra-lake processes. The influx of reworked tephra-derived glass shards from the catchment is mainly seen in the detrital winter layers starting directly after the ash fall and can last at least 1240 years following the primary tephra deposition (e.g., TM-18/CI). The highest concentrations of reworked glass shards occur during the first four years following deposition and exponentially decrease during the following years (Table 3). The duration of this influx and the amount of reworked tephra-derived material strongly depends on the thickness (volume) of the primary tephra deposit (Table 3). The duration for tephra re-deposition varies from six years for the thinnest tephra, TM-18-2 (1 mm), up to several decades for the TM-18-1 tephras (5-32 mm), and even >1240 years for the thickest TM-18/CI deposit (230 mm). For the youngest and relative thick TM-17-2/Schiava tephra (20 mm), scattered reworked material can be observed only up to 10 years after primary deposition indicating less erosion in the catchment probably as a consequence of a more stable vegetation cover during this time interval at Monticchio.

The lake ecosystem itself showed a direct response to tephra deposition visible by significant increases in the thickness of planktonic diatom layers for up to the ten years after the primary fallout of tephras TM-17-2, TM-18/CI, TM-18-1a, TM-18-1c, and TM-18-1d (Table 3). The thinnest tephra TM-18-2, as well as TM-18-1b (not visible because of homogenous and bioturbated sediments), did not show an obvious change to the diatom population. Elevated diatom productivity after major ash falls is consistent with other findings, for example in central-northern Europe and Northern America. Birks and Lotter (1994) and De Klerck et al. (2008), for example, described an increase of the diatom productivity after the deposition of the Laacher See Tephra (Eifel Volcanic Field) in Late Allerød sediments of distal lakes. A similar diatom response was observed after the deposition of relative thick tephras (>1 cm) in lakes in British Columbia (Hickmann and Reasoner, 1994) and Mexico (Telford et al., 2004).

The increase in diatoms is interpreted as a consequence of an additional input of silica from the rapid dissolution of volcanic glass shards, which is a major nutrient source for building diatom frustules (Hickmann and Reasoner, 1994; De Klerck et al., 2008). An increase in diatom production is visible for a time period of 5 to 20 years after the deposition of the Laacher See Tephra (Birks and Lotter, 1994) and encompasses a period of several hundred years in the Canadian lakes (Hickmann and Reasoner, 1994). A study from New Zealand at Lake Poukawa, numbers of diatoms per unit dry weight increased, but the proportion of epiphytic species decreased immediately after tephra-fall into the lake (Harper et al., 1986). The tephra layers possibly preserved more diatom frustules, or increased diatom growth by supplying silica, phosphorus, and sulphur nutrients directly, or organic matter from vegetation damage in the surrounding catchment.

5.2 The Campanian Ignimbrite and its role as a chronostratigraphic marker in the Mediterranean area

The Campanian Ignimbrite is one of the most widespread tephra deposits in the Mediterranean and therefore ideal for linking terrestrial and marine archives in this region. However, as inferred from the Monticchio tephra sequence, the CI eruption was preceded by at least four smaller-scale explosive eruptions ("CI-like" tephras TM-18-1) that derived most likely from the same volcanic source (Phlegrean Fields). These eruptions occurred within a time period of ca. 600 varve years prior to the CI, and TM-18-1 tephras are geochemically difficult to distinguish from the CI and from one other without high-precision trace element glass data. Thus, to avoid miscorrelation, a careful inspection of tephras is required prior to using the CI for the synchronisation of last glacial palaeoenvironmental records. The CI in the Monticchio sequence (TM-18) is a very thick, coarse grained fall- and co-ignimbrite deposit that has been unambiguously identified on the basis of its lithological composition in the proximal-medial area. Because of the magnitude of the CI eruption, occurrences of the CI at further distal and ultra-distal sites within the main easterly dispersal axis (see overview in Pyle et al., 2006) are supposed to correlate with both the CI fallout and tephra TM-18 in the Monticchio record. However, correlations can be difficult in medial-distal sites in the central Mediterranean area. Here, the less widely dispersed "CI-like" tephras can occur in addition to the CI in high-resolution terrestrial and marine records (i.e., Adriatic Sea; Bourne et al., 2010), or form a mixed layer in lower-resolution deep-sea records of the Ionian and Tyrrhenian Seas (i.e., tephra C-13; Paterne et al., 1986, 1988). In these cases, synchronisation of records

requires the identification of other geochemically distinct tephras such as the Schiava tephra from Vesuvius.

The tephra links between the Monticchio record and distal to ultra-distal sites in the eastern Mediterranean area is less problematic (Fig. 10a). Tephra layers investigated in this study deposited during the stadial between Greenland Interstadials GI-9 and GI-8 (tephras TM-18 to TM-18-2), which has been associated with the Heinrich H4-event (Svensson et al., 2008), and at the onset of GI-8 (tephra TM-17-2) (Fig. 2, Fig. 10a). The transition from stadial to interstadial conditions at Monticchio is well documented by the distinct lithological changes in the sediments. Stadial sediments are characterised by a higher detrital influx (turbidites), a lack of calcite precipitates, lower diatom concentrations and generally poorer varve preservation than that associated with interstadial conditions. These features together are interpreted as caused by cooler temperatures, lower bioproductivity, oxygen-rich lake bottom conditions (allowing bioturbation to occur) and reduced vegetation cover in the catchment. The interstadial sediments, however, reveal a lower detrital input and larger amounts of diatoms and autochthonous calcite layers, pointing to a general higher bioproductivity and probably warmer climatic conditions correlating with GI-8. In addition, varves are well preserved in this interval indicating anoxic lake bottom conditions prevailed and hence bioturbation was minimised (Fig. 10b). These sedimentological changes are accompanied by a change in pollen, for example a decrease of steppe pollen that is dated in Monticchio at 35,607 ± 1780 varve years BP and might correlate to GI-8 (Fig. 10a). This varve age, however, may require a correction since the CI in Monticchio is 2506 years too young (36,774 varve years) compared with its well accepted $^{40}Ar/^{39}Ar$ age (39,280 ± 110 yrs BP; De Vivo et al., 2001). Accordingly, the corrected age of GI-8 onset in Monticchio would lay at c. 38,110 varve years BP. The onset of interstadial conditions in Monticchio is dated at 1167 years after the CI eruption and 76 years prior to the Schiava eruption, and 2613 years younger than the onset of GI-8 in Greenland (38,220 ± 725 yrs b2k; Svensson et al., 2008). This discrepancy is most likely due to the above mentioned underestimation of the Monticchio varve-based chronology for this interval. Because of the absence of a common marker in the Greenland ice core and Monticchio records it is not possible to investigate potential leads and lags between these regions for this transition, so far.

Comparisons with other high-resolution archives in the eastern Mediterranean area, such as the peat sequence of Tenaghi Philippon (Greece) and the Black Sea sediment sequence M72-5-24-GC3, rely on the CI as synchronisation marker (Fig. 10). Proxy data of both sequences recorded stadials and interstadials during MIS 3 similar to those of the Monticchio record. For

the Black Sea sediments, which are dated by a combination of radiocarbon dating and tuning to the NGRIP oxygen isotope record, these climatic variations are best demonstrated by the calcium record interpreted as temperature proxy (Nowaczyk et al., 2012). Here, the onset of interstadial conditions correlated to GI-8 is dated 1110 years after the deposition of the CI which is in agreement with the timing in Monticchio (1167 varve years). In the Tenaghi Philippon record a strong decline of steppe pollen (Müller et al., 2011) is independently radiocarbon dated to occur 1400 years after the CI. Here, it appears that the apparent 230-year difference in the duration of the interval from the CI eruption to the onset of interstadial conditions in Monticchio and Tenaghi Philippon is more likely due to dating differences between the Tenaghi radiocarbon ages and the Monticchio differential varve counts.

In all three Mediterranean records, Monticchio, Tenaghi Philippon and Black Sea the CI is occurs clearly 700-800 years after the onset of a millennial-scale cold stadial correlated to H4 at c. 40,100 cal years BP (Fig. 10). This finding is consistent with other terrestrial high resolution palaeo-records where the CI has been described (e.g., Margari et al., 2009; Lowe et al., 2012). This stratigraphic juxtaposition clearly rules out that the CI eruption has triggered or accelerated this Northern-hemispheric climatic cooling as suggested by Fedele et al. (2002, 2008). At Lago Grande di Monticchio, the fallout of thick deposits of the CI tephra distinctly influenced the erosional and depositional system of the lake and its catchment for several centuries to millennia.

6. Conclusions

Analyses of seven tephras in the time interval of 40-38 ka BP in the sediment record of Lago Grande di Monticchio revealed several implications for future palaeoclimate and palaeoenvironmental research.

- The varved Monticchio sediment sequence is a unique recorder of distal tephra deposition, providing clear stratigraphic order and precise dating of tephra events especially for closely timed eruptions that are difficult to decipher in proximal records.
- The deposition of distal fallout tephras in the lake sediments of Lago Grande di Monticchio particularly during cold stadial conditions had an environmental impact, mainly recorded as increased reworking processes of tephra materials (mainly glass shards). Reworking of tephra material from the catchment occurs over several years for thin tephras (<1 mm thickness) and over decades and >1240 years for the thicker tephra deposits (>5 mm).

- Microfacies analyses have demonstrated that the sediments of Monticchio are characterised not only by the deposition of numerous primary tephra fall deposits but also that this material is incorporated in the annual deposition cycle particularly after ash falls as it occurs as a major component in the detrital winter layers. This fact complicates the search for additional cryptotephras of other eruptions within the Lago Grande di Monticchio sequence.
- Significant increases in the thickness of planktonic diatom layers are visible up to ten years after the deposition of thicker (>1 mm), primary tephra layers, while diatom populations show no obvious response after the deposition of thinner tephras in the Monticchio record.
- The Campanian Ignimbrite eruption was preceded by at least four tephra-generating eruptions of the Phlegrean Fields occurring within a time period of approximately 600 years. These four tephras and the CI show a similar major and minor element glass composition, but are clearly distinguishable by their trace elemental glass compositions. Synchronisation of last glacial palaeoenvironmental records thus requires a careful inspection prior to use Campanian tephras.
- Despite apparent differences in varve-based ages from the Monticchio record compared to the Black Sea or Tenaghi Philippon records, differential dating in intervals with tephra marker layers like the CI and the Schiava pumices allows to determine the length of the H4 stadial, which is c. 2000 years in Monticchio. In particular, the Schiava pumices dated at 35,530 varve years BP (corresponding to a corrected age of 38,040 years BP) provides an excellent marker tephra layer for the GI-9/GI-8 time interval because of their distinct geochemistry and their close position to the GI-8/H4 transition.
- Using the $^{40}Ar/^{39}Ar$ age of the CI as a temporal anchor point, the onsets of the H4-stadial and GI-8 interstadial are dated at 40,100 and 38,110 cal years BP in the Monticchio record.

7. Acknowledgements

We thank Gabi Arnold and Michael Köhler for thin section preparation of tephra samples and Oona Appelt for technical support during EPMA analyses. We are very grateful to Dr. Roberto Sulpizio and an anonymous reviewer for helpful and constructive comments on the manuscript. This manuscript is a contribution to the climate initiative REKLIM Topic 8 ‘Abrupt climate change derived from proxy data’ of the Helmholtz Association, the INTIMATE EU-COST Action ES0907, and the RESET (Response of Humans to Abrupt Environmental Transitions) programme funded by the NERC.

8. References

Alessio, M., Bella, F., Improta, S., Belluomini, G., Calderoni, G., Cortesi, C., Turi, B., 1976. University of Rome Carbon-14 dates XIV. Radiocarbon 18, 321 - 349.

Allen, J.R.M., Brandt, U., Brauer, A., Hubberten, H.-W., Huntley, B., Keller, J., Kraml, M., Mackensen, A., Mingram, J., Negendank, J.F.W., Nowaczyk, N.R., Oberhänsli, H., Watts, W.A., Wulf, S., Zolitschka, B., 1999. Rapid environmental changes in southern Europe during the last glacial period. Nature 400, 740-743.

Andersen, K. K., Svensson, A., Rasmussen, S. O., Steffensen, J. P., Johnsen, S. J., Bigler, M., Röthlisberger, R., Ruth, U., Siggaard-Andersen, M.-L., Dahl-Jensen, D., Vinther, B. M., Clausen, H. B., 2006. The Greenland Ice Core Chronology 2005, 15–42 ka. Part 1: constructing the time scale, Quaternary Science Reviews 25, 3246–3257.

Barberi, F., Innocenti, F., Lirer, L., Munno, R., Pescatore, T., Santacroce, R., 1978. The Campanian Ignimbrite: a major prehistoric eruption in the Neapolitan Area (Italy). Bulletin of Volcanology 41, 10 - 31.

Birks, H.J.B., Lotter, A.F., 1994. The impact of the Laacher See volcano (11000 yr B.P.) on terrestrial vegetation and diatoms. Journal of Paleolimnology 11, 313 - 322.

Bourne, A.J., Lowe, J.J., Trincardi, F., Asioli, A., Blockley, S., Wulf, S., Matthews, I.P., Piva, A., Vigliotti, L., 2010. Distal tephra record for the last ca 105,000 years from core PRAD 1-2 in the central Adriatic Sea: implications fro marine tephrostratigraphy. Quaternary Science Reviews 29, 3079-3094.

Brandt, U., Nowaczyk, N.R., Ramrath, A., Brauer, A., Mingram, J., Wulf, S., Negendank, J.F.W., 1999. Palaeomagnetism of Holocene and Late Pleistocene sediments from Lago di Mezzano and Lago Grande di Monticchio (Italy): initial results. Quaternary Science Reviews 18, 961-976.

Brauer, A., Allen, J.R.M., Mingram, J., Dulski, P., Wulf, S., Huntley, B., 2007. Evidence for last interglacial chronology and environmental change from Southern Europe. PNAS 104, 450-455.

Brauer, A., Mingram, J., Frank, U., Günter, C., Schettler, G., Wulf, S., Zolitschka, B., Negendank, J.F.W., 2000. Abrupt environmental oscillations during the Early Weichselian recorded at Lago Grande di Monticchio, southern Italy. Quarternary International 73/74, 79-90.

Brocchini, D., La Volpe, L., Laurenzi, M.A., Principe, C., 1994. Storia evolutiva del Monte Vulture. Plinius 12, 22-25.

Brown, R.J., Orsi, G., de Vita, S., 2008. New insights into Late Pleistocene explosive volcanic activity and caldera formation on Ischia (southern Italy). Bulletin of Volcanology 70, 583-603.

D'Antonio, M., Civetta, L., Orsi, G., Pappalardo, L., Piochi, M., Carandente, A., de Vita, S., Di Vito, M.A., Isaia, R., 1999. The present state of the magmatic system of the Campi Flegrei caldera based on a reconstruction of its behavior in the past 12 ka. Journal of Volcanology and Geothermal Research 91, 247-268.

Damaschke, M., Sulpizio, R., Zanchetta, G., Wagner, B., Böhm, A., Nowaczyk, N., Rethemeyer, J., Hilgers, A., 2013. Tephrostratigraphic studies on a sediment core from Lake Prespa in the Balkans. Climate of the Past 9, 267-287.

De Klerck, P., Janke, W., Kühn, P., Theuerkauf, M., 2008. Environmental impact of the Laacher See eruption at large distance from the volcano: integrated palaeoecological studies from Vorpommern (NE Germany). Palaeogeography, Palaeoclimatology, Palaeoecology 270, 196-214.

De Vivo, B., Rolandi, G., Gans, P.B., Calvert, A., Bohrson, W.A., Spera, F.J., Belkin, H.E., 2001. New constraints on the pyroclastic eruptive history of the Campanian volcanic plain (Italy). Mineral. Petrol. 73, 47-65.

Di Renzo, V., Di Vito, M.A., Arienzo, I., Carandente, A., Civetta, L., D'Antonio, M., Giordano, F., Orsi, G., Tonarini, S., 2007. Magmatic history of Somma-Vesuvius on the basis of new geochemical and isotopic data from a deep borehole (Camaldoli della Torre). Journal of Petrology 48, 753-784.

Di Vito, M.A., Sulpizio, R., Zanchetta, G., D'Orazio, M., 2008. The late Pleistocene pyroclastic deposits of the Campanian Plain: New insights into the explosive activity of Neapolitan volcanoes. Journal of Volcanology and Geothermal Research 177, 19-48.

Druitt, T.H., Edwards, L., Mellors, R.M., Pyle, D.M., Sparks, R.S.J., Lanphere, M., Davies, M., Barriero, B., 1999. Santorini Volcano. Geological Society, London.

Fedele, F.G., Giaccio, B., Hajdas, I., 2008. Timescales and cultural process at 40,000 BP in the light of of the Campanian Ignimbrite eruption, Western Eurasia. Journal of Human Evolution 55, 834-857.

Fedele, F.G., Giaccio, B., Isaia, R., Orsi, G., 2002. Ecosystem impact of the Campanian Ignimbrite eruption in Late Pleistocene Europe. Quaternary Research 57, 420-424.

Giaccio, B., Isaia, R., Fedele, F.G., Di Canzio, E., Hoffecker, J., Ronchitelli, A., Sinitsyn, A.A., Anikovich, M., Lisitsyn, S.N., Popov, V.v., 2008. The Campanian Ignimbrite and Codola tephra layers: Two temporal/stratigraphic markers for the Early Upper Palaeolithic in southern italy and eastern Europe. Journal of Volcanology and Geothermal Research 177, 208-226.

Harper, M.A., Howorth, R., McLeod, M., 1986. Late Holocene diatoms in Lake Poukawa: effects of airfall tephra and changes in depth. New Zealand Journal of Marine and Freshwater Research 20, 107-118.

Hickmann, M., Reasoner, M., 1994. Diatom responses to late Quaternary vegetation and climate change, and to deposition of two tephras in an alpine and sub-alpine lake in Yoho National Park, British Colombia. Journal of Paleolimnology 11, 173-188.

Hunt, J.B., Hill, P.G., 1996. An inter-laboratory comparison of the electron probe microanalysis of glass geochemistry. Quaternary International 34-36, 229-241.

Keller, J., Ryan, W.B.F., Ninkovich, D., Altherr, R., 1978. Explosive volcanic activity in the Mediterranean over the past 200,000 yr as recorded in deep-sea sediments. Geological Society of America Bulletin 89, 591 - 604.

Kuehn SC, Froese DG, Shane PAR, and Intercomparison Participants (INTAV), 2011. The INTAV intercomparison of electron-beam microanalysis of glass by tephrochronology laboratories: results and recommendations. Quaternary International 246, 19–47.

Kylander, M.E., Lind, E.M., Wastegard, S., Löwemark, L., 2011. Recommendations for using XRF core scanning as a tool in tephrochronology. The Holocene 22, 371-375.

Laurenzi, M.A., Brocchini, D.I., Principe, C., Ferrara, G., 1993. Mt.Vulture volcano chronostratigraphy and the effectiveness of dating young phlogopites. Terra abstracts 5, 572-573.

Le Bas, M.J., Le Maitre, R.W., Streckeisen, A., Zanettin, B., 1986. A chemical classification of volcanic rocks based on the Total Alkali-Silica diagram. Journal of Petrology 27, 745 - 750.

Lowe, D.J., 2011. Tephrochronology and its application: a review. Quaternary Geochronology 6, 107–153.

Lowe, J., Barton, N., Blockley, S.P.E., Bronk Ramsey, C., Cullen, V.L., Davies, W., Gamble, C., Grant, K., Hardiman, M., Housley, R., Lane, C.S., Lee, S., Lewis, M., Macleod, A., Menzies, M., Müller, W., Pollard, M., Price, C., Roberts, A.P., Rohling, E.J., Satow, C., Smith, V.C., Stringer, C.B., Tomlinson, E.L., White, D., Albert, P., Arienzo, I., Barker, G., Bori_c, D., Carandente, A., Civetta, L., Ferrier, C., Guadelli, J.L., Karkanas, P., Koumouzelis, M., Müller, U.C., Orsi, G., Pross, J., Rosi, M., Shalamanov-Korobar, L., Sirakov, N., Tzedakis, P.C., 2012. Volcanic ash layers illuminate the resilience of Neanderthals and early modern humans to natural hazards. Proceedings of the National Academy of Sciences 109, 13532-13537.

Lowe, J.J., Blockley, S., Trincardi, F., Asioli, A., Cattaneo, A., Matthews, I.P., Pollard, M., Wulf, S., 2007. Age modelling of late Quaternary marine sequences in the Adriatic: Towards improved precision and accuracy using volcanic event stratigraphy. Continental Shelf Research 27, 560-582.

Margari, V., Gibbard, P.L., Bryant, C.L., Tzedakis, P.C., 2009. Character of vegetational and environmental changes in southern Europe during the last glacial period; evidence from Lesvos Island, Greece. Quaternary Science Reviews 28, 1317-1339.

Matthes, S., 1999. Mineralogie - Eine Einführung in die spezielle Mineralogie, Petrologie und Lagerstättenkunde. Springer Verlag, Berlin.

Müller, U.C., Pross, J., Tzedakis, P.C., Gamble, C., Kotthoff, U., Schmiedl, G., Wulf, S., Christanis, K., 2011. The role of climate in the spread of modern humans into Europe. Quaternary Science Reviews 30, 273-279.

Munno, R., Petrosini, P., 2007. The late Quaternary tephrostratigraphical record of the San Gregorio Magno basin (southern Italy). Journal of Quaternary Science 22, 247-266.

Narcisi, B., 1996. Tephrochronology of a late quaternary lacustrine record from the Monticchio Maar (Vulture Volcano, southern Italy). Quaternary Science Reviews 15, 155 - 165.

Narcisi, B., Vezzoli, L., 1999. Quaternary stratigraphy of distal tephra layers in the Mediterranean - an overview. Global and Planetary Change 21, 31-50.

NGRIP members, 2004. High-resolution record of Northern Hemisphere climate extending into the last interglacial period. Nature 431(7005), 147-151

Nowaczyk, N.R., Arz, H.W., Frank, U., Kind, J., Plessen, B., 2012. Dynamics of the Laschamp geomagnetic excursion from Black Sea sediments. Earth and Planetary Science Letters 351-352, 54-69.

Ort, M., Orsi, G., Pappalardo, L., Fisher, R.V., 2003. Anisotropy of magnetic susceptibility studies of depositional processes in the Campanian Ignimbrite, Italy. Bulletin of Volcanology 65, 55-72.

Pappalardo, L., Civetta, L., D' Antonio, M., Deino, A., Di Vito, M., Orsi, G., Carandente, A., de Vita, S., Isaia, R., Piochi, M., 1999. Chemical and Sr-isotopical evolution of the Phlegrean magmatic system before the Campanian Ignimbrite and the Neapolitan Yellow Tuff eruptions. Journal of Volcanology and Geothermal Research 91, 141-166.

Paterne, M., Guichard, F., 1993. Triggering of volcanic pulses in the Campanian area, South Italy, by periodic deep magma influx. Journal of Geophysical Research 98, 1861 - 1873.

Paterne, M., Guichard, F., Labeyrie, J., 1988. Explosive activity of the South Italian volcanoes during the past 80,000 years as determined by marine tephrochronology. Journal of Volcanology and Geothermal Research 34, 153-172.

Paterne, M., Guichard, F., Labeyrie, J., Gillot, P.Y., Duplessy, J.C., 1986. Tyrrhenian Sea tephrochronology of the oxygen isotope record for the past 60,000 years. Marine Geology 72, 259 - 285.

Peccerillo, A., 2005. Plio-Quaternary volcanism in Italy. Petrology Geochemistry. Geodynamics, Springer, Heidelberg, 1–365.

Poli, S., Chiesa, S., Gillot, P.-Y., Gregnanin, A., Guichard, F., 1987. Chemistry versus time in the volcanic complex of Ischia (Gulf of Naples, Italy): evidence of successive magmatic cycles. Contributions to Mineralogy and Petrology 95, 322 - 335.

Poli, S., Chiesa, S., Gillot, P.-Y., Guichard, F., Vezzoli, L., 1989. Time dimension in the geochemical approach and hazard estimates of a volcanic area: the Isle of Ischia case (Italy). Journal of Volcanology and Geothermal Research 36, 327 - 335.

Pyle, D.M., Ricketts, G.D., Margari, V., van Andel, T.H., Sinitsyn, A.A., Praslov, N.D., Lisitsyn, S., 2006. Wide dispersal and deposition of distal tephra during the Pleistocene 'Campanian Ignimbrite/Y5' eruption, Italy. Quaternary Science Reviews 25, 2713-2728.

Rosi, M., Vezzoli, L., Castelmenzano, A., Grieco, G., 1999. Plinian pumice fall deposit of the Campanian Ignimbrite eruption (Phlegraean Fields, Italy). Journal of Volcanology and Geothermal Research 91, 179-198.

Santacroce, R., Cioni, R., Marianelli, P., Sbrana, A., Sulpizio, R., Zanchetta, G., Donahue, D.J., Joron, J.L., 2008. Age and whole rock-glass compositions of proximal pyroclastics from the major explosive eruptions of Somma-Vesuvius: A review as atool for distal tephrostratigraphy. Journal of Volcanology and Geothermal Research 177, 1-18.

Shane, P.A.R., Nairn, I.A., Martin, S.B., Smith, V.C., 2008. Compositional heterogeneity in tephra deposits resulting from the eruption of multiple magma bodies: implications for tephrochronology. Quaternary International 178, 44-53.

Siani, G., Sulpizio, R., Paterne, M., Sbrana, A., 2004. Tephrostratigraphy study for the last 18,000 ^{14}C years in a deep-sea sediment sequence for the South Adriatic. Quaternary Science Reviews 23, 2485-2500.

Sulpizio, R., Zanchetta, G., D'Orazio, M.D., Vogel, H., Wagner, B., 2010. Tephrostratigraphy and tephrochronology of lakes Ohrid and Prespa, Balkans. Biogeosciences Discussions 7, 3931-3967.

Sulpizio, R., Zanchetta, G., Paterne, M., Siani, G., 2003. A review of tephrostratigraphy in central and southern Italy during the last 65 ka. Il Quaternario 16, 91-108.

Svensson, A., Andersen, K.K., Bigler, M., Clausen, H.B., Dahl-Jensen, D., Davies, S.M., Johnsen, S.J., Muscheler; R., Parrenin, F., Rasmussen, S.O., Röthlisberger, R., Seierstad, I., Steffensen, J.P., Vinther, B.M., 2008. A 60000 year Greenland stratigraphic ice core chronology. Climate of the Past 4, 47-57.

Telford, R.J., Barker, P., Metcalfe, S., Newton, A.J., 2004. Lacustrine responses to tephra deposition: examples from Mexico. Quaternary Science Reviews 23, 2337-2353.

Thunell, R., Williams, D., Tappa, E., Rio, D., Raffi, I., 1979. The age, origin and volcanological significance of the Y-5 ash layer in the Mediterranean. Quaternary Research 12, 241-253.

Tomlinson, E.L., Arienzo, I., Civetta, L., Wulf, S., Smith, V.C., Hardiman, M., Lane, C.S., Carandente, A., Orsi, G., Rosi, M., Müller, W., Menzies, M.A., 2012. Geochemistry of the Phlegrean Fields (Italy) proximal sources for major Mediterranean tephras: Implications for the dispersal of Plinian and co-ignimbritic components of explosive eruptions. Geochimica et Cosmochimica Acta 93, 102-128.

Tomlinson, E.L., Thordarson, T., Müller, W., Thirlwall, M.F., Menzies, M.A., 2010. Micro analysis of tephra by LA-ICP-MS - strategies, advantages and limitations assessed using the Thorsmork ignimbrite (Southern Iceland). Chemical Geology 279, 73-89.

Vezzoli, L., 1988. Island if Ischia. CNR, Roma.

Vezzoli, L., 1991. Tephra layers in Bannock Basin (Eastern Mediterranean). Marine Geology 100, 21 - 34.

Watts, W.A., Allen, J.R.M., Huntley, B., 1996. Vegetation history and palaeoclimate of the last glacial period at Lago Grande di Monticchio, southern Italy. Quaternary Science Reviews 15, 133-153.

Wulf, S., Brauer, A., Kraml, M., Keller, J., Negendank, J.F.W., 2004. Tephrochronology of the 100 ka lacustrine sediment record of Lago Grande di Monticchio (southern Italy). Quaternary International 122, 7-30.

Wulf, S., Brauer, A., Mingram, J., Zolitschka, B., Negendank, J.F.W., 2006. Distal tephras in the sediments of Monticchio maar lakes, In: Principe, C. (Ed.), La geologia del monte Vulture. Consiglio Nazionale delle Ricerche, pp. 105-122.

Wulf, S., Keller, J., Paterne, M., Mingram, J., Lauterbach, S., Opitz, S., Sottili, G., Giaccio, B., Albert, P.G., Satow, C., Tomlinson, E.L., Viccaro, M., Brauer, A., 2012. The 100-133 ka record of Italian explosive volcanism and revised tephrochronology of Lago Grande di Monticchio. Quaternary Science Reviews 58, 104-123.

Wulf, S., Kraml, M., Keller, J., 2008. Towards a detailed distal tephrostratigraphy in the Central Mediterranean: The last 20,000 yrs record of Lago Grande di Monticchio. Journal of Volcanology and Geothermal Research 2008, 118-132.

Wulf, S., Ott, F., Slowinski, M., Noryskiewicz, A.M., Dräger, N., Martin-Puertas, C., Czymzik, M., Neugebauer, I., Dulski, P., Bourne, A.J., Blaszkiewicz, M., Brauer, A., 2013. Tracing the Laacher See Tephra in the varved sediment record of the Trzechowskie palaeolake in central Northern Poland. Quaternary Science Reviews 76, 129-139.

Zolitschka, B., 1990. Jahreszeitlich geschichtete Seesedimente ausgewählter Eifelmaare. Documenta naturae 60, 1-226.

Zolitschka, B., Negendank, J.F.W., 1996. Sedimentology, dating and palaeoclimatic interpretation of a 76.3 ka record from Lago Grande di Monticchio, southern Italy. Quaternary Science Reviews 15, 101 - 112.

Table captions

Table 1: Ages, compositions, and sources of seven tephras in Monticchio sediments aged 40-38 ka. Abbreviations: m = minerals; j = juvenile clasts (glass shards, pumice fragments). Ages of tephras are provided by the varve chronology of Monticchio sediments after Brauer et al. (2007). [1]A mean counting error of 5% has been estimated for the Monticchio varve-based chronology (Wulf et al., 2012). *Corrected ages were calculated by incremental dating (varve counts in between tephras) using the $^{40}Ar/^{39}Ar$ age of 39.28 ± 0.11 ka BP of the CI (De Vivo et al., 2001) as a fixed age. For references see text.

Table 2: Mean values and standard deviations (given in parentheses) of the non-normalised major element glass composition of the tephra layers analysed by EPMA-WDS in the Lago Grande di Monticchio. Single analyses are provided in Supplementary File 1. N = number of analysed glass shards. Total $_{corr.}$ = totals corrected for oxid values of Cl and F. * Data from Wulf et al. (2004).

Table 3: Characteristics of tephra layers investigated in this study (thicknesses and µ-XRF elemental signals), and sedimentological and ecological response times and processes after primary tephra deposition. * Enclosing tephra sediments (see text).

Figure captions

Figure 1: Location of Lago Grande di Monticchio, Italian volcanic centres and sites mentioned in the text of tephra correlatives.

Figure 2: Lithology, magnetic susceptibility (data from Brandt et al., 1999), µ-XRF elemental composition (K, Si, Ca, Mn and Ti), and positions of tephra layers in the sediment section 40-38 ka from Lago Grande di Monticchio.

Figure 3: **(A)** Large-scale thin section image (polarised light) of tephra TM-17-2 (Schiava tephra) and enclosing varved sediments. **(B)** Microscopic images of tephra components under polarised (left) and transmitted light (right). Vg = volcanic glass, cpx = clinopyroxene, kf = potassium feldspar (sanidine), dc = detrital carbonate, io = Fe-Ti oxide. **(C)** Polarised light image of several L4 varves. **(D)** Transmitted light image of the structure of a typical L4 varve.

Figure 4: Photograph of core LGM-J11-o, 83-92 cm **(A)** and transmitted light image **(B)** showing the Ischia tephra TM-18-2 within varved L2 sediments. **(C)** Structure and composition of several L2 varves.

Figure 5: Biplots for discriminating and comparing Monticchio tephras TM-17-2 to TM-18-2 to proximal and distal potential correlative on the basis of major element glass compositional (water-free) data. **(A)** Total-alkali-silica diagram SiO_2 versus K_2O+Na_2O after (Le Bas et al., 1986). **(B)** SiO_2 concentration versus alkali ratio K_2O/Na_2O. **(C)** FeO versus CaO (wt%). Data for comparison are from: (1) EPMA glass data (Damaschke et al., 2013); (2) EPMA glass data (Tomlinson et al., 2012); (3) EPMA glass data (Sulpizio et al., 2010); (4) EPMA glass data (Bourne et al., 2010); (5) XRF bulk pumice data (Vezzoli, 1988); (6) ICP-AES bulk glass data and SEM-EDS single grain data (Di Vito et al., 2008); (7) ICP-AES bulk glass data (Di Renzo et al., 2007); (8) mean of SEM-EDS glass data (Paterne et al., 1988); (9) ICP-AES bulk glass data (Pappalardo et al., 1999).

Figure 6: **(A)** Photograph of core LGM-J10-u at depth 28.5-74.5 cm showing the sub-layers of tephra TM-18 (Campanian Ignimbrite, CI) as explained in the text and enclosing sediments. **(B)** Microscopic images of tephra components from (1) the base of TM-18, (2) the middle of unit LFU (lower fall unit), and (3) the top of unit UFU (upper fall unit).

Figure 7: **(A)** Photograph of core LGM-J10-u at depth 71-94 cm showing the position of tephras TM-18-1a and TM-18-1b within laminated sediments below the CI/TM-18 tephra. **(B)** Brown glass shard enriched in apatite microcrystals in tephra TM-18-1a. **(C)** Microscopic image (transmitted light) of brown and colourless glass shards of tephra TM-18-1b.

Figure 8: Biplots of trace element single glass compositions for **(A)** discriminating Monticchio tephras TM-18 (CI), TM-18-1a, TM-18-1b, TM-18-1c, and TM-18-1d and **(B)** comparing those tephras with ICP-AES bulk glass data from proximal and medial-distal tephra deposits. Data from: (1) single grain data (Tomlinson et al., 2012); (2) ICP-MS bulk glass data (Di Vito et al., 2008); (3) ICP-MS bulk glass data (Pappalardo et al., 1999).

Figure 9: **(A)** Core photograph of LGM-M12-o at 58-71 cm showing the position of tephra TM-18-1c and a microscopic transmitted light image of tephra components. **(B)** Photograph of core LGM-M12-u at depth 0-21.5 cm with tephra TM-18-1d at the top and microscopic image of glass shards.

Figure 10: **A)** Comparison of proxy records from the eastern Mediterranean area for the time interval 25-50 cal ka BP and tephra synchronisation. Note that the pollen records from Lago Grande di Monticchio and Tenaghi Philippon are plotted against their own time scales. The varve-based age chronology of the Monticchio record (published by Brauer et al., 2007) (left scale) has been additionally corrected for this study by +2506 varve years (right scale) by tuning to the $^{40}Ar/^{39}Ar$ age of 39.28 ± 0.11 of the Campanian Ignimbrite (CI) (De Vivo et al., 2001). Orange bars below the CI in the Monticchio record indicate the positions of tephras TM-18-1 a-d and TM-18-2. The age model of the Tenaghi Philippon pollen record is based on radiocarbon dates. Black Sea cores M72-5-24-GC3 are both independently dated by ^{14}C and the Ca-record tuned to Greenland ice core NGRIP. Grey bars indicate the position of the Heinrich H4-event. GI = Greenland Interstadial. **B)** Scan of the sediment block of section LGM-M10-u at depth 69-79 cm (upper photograph) and transmitted light microscopic image

(lower photograph) showing the transition from homogeneous H4-stadial sediments to well-laminated GI-8 sediments in the Monticchio record.

Supplementary Files

Supplementary File 1: Electron microprobe data (not normalised) of individual glass shards of Monticchio tephras and the Lipari reference glass standard.

Supplementary File 2: Images and µ-XRF elemental data of analysed cores showing the position of primary and reworked tephra layers.

Table 1

Tephra	**Age (varve yrs BP) and 5% counting error[1]**	**Interpolated varve age (yrs BP)***	**Maximum grain sizes $d_{max.}$ (µm)**	**Source volcano**	**Correlatives**
TM-17-2	35,530 ± 1780	38,040	250 (j), 600 (m)	Vesuvius	Schiava Pumices, C-9
TM-18	36,770 ± 1840	39,280 ± 110	(V7): 600 (j) (V6): 1000 (j) (V5): 1100 (j) (V4): 800 (j) (V3): 8000 (j) (V2): 2800 (j) (V1): 1800 (j)	Phlegrean Fields	Campanian Ignimbrite, C-13
TM-18-1a	36,840 ± 1840	39,350	450 (j), 150 (m)	Phlegrean Fields	C-13?, PT0915-8?, PRAD1752?
TM-18-1b	36,950 ± 1850	39,460	150 (j+m)	Phlegrean Fields	PT0915-8? PRAD1752?
TM-18-1c	37,060 ± 1850	39,570	600 (j), 50 (m)	Phlegrean Fields	PT0915-8? PRAD1752?
TM-18-1d	37,360 ± 1870	39,870	300 (j+m)	Phlegrean Fields	SMP1-a, PT0915-8?, PRAD1752?
TM-18-2	37,590 ± 1880	40,100	250 (j), 230 (m)	Ischia	Citara Formation, C-14

Table 2

Sample	TM-17-2	TM-18*		TM-18-1a	TM-18-1b	TM-18-1c	TM-18-1d		TM-18-2
No. Anal.	**N = 9**	**N = 42**	**N = 1**	**N = 10**	**N = 7**	**N = 6**	**N = 13**	**N = 1**	**N = 11**
SiO_2	62.77 (1.03)	61.15 (0.94)	59.30	60.20 (0.82)	59.35 (0.56)	59.72 (0.74)	59.66 (0.76)	58.59	63.24 (0.46)
TiO_2	0.38 (0.10)	0.42 (0.02)	0.43	0.40 (0.03)	0.44 (0.02)	0.42 (0.02)	0.44 (0.02)	0.49	0.48 (0.02)
Al_2O_3	17.16 (0.82)	18.95 (0.38)	18.87	18.70 (0.26)	18.53 (0.20)	18.51 (0.28)	18.86 (0.23)	18.50	18.31 (0.17)
FeO	2.19 (0.37)	2.91 (0.10)	3.16	2.66 (0.26)	2.90 (0.24)	2.82 (0.04)	2.95 (0.09)	3.70	2.42 (0.10)
MnO	0.13 (0.04)	0.24 (0.02)	0.17	0.22 (0.03)	0.23 (0.02)	0.24 (0.02)	0.26 (0.01)	0.15	0.18 (0.03)
MgO	0.25 (0.08)	0.35 (0.02)	0.51	0.31 (0.03)	0.36 (0.06)	0.34 (0.01)	0.32 (0.01)	1.00	0.33 (0.04)
CaO	2.49 (0.53)	1.72 (0.08)	2.28	1.76 (0.10)	1.70 (0.10)	1.70 (0.03)	1.68 (0.04)	3.04	1.40 (0.08)
Na_2O	3.34 (0.20)	5.60 (0.70)	4.83	5.80 (0.16)	5.82 (0.31)	5.79 (0.20)	6.34 (0.19)	3.93	5.41 (0.38)
K_2O	7.59 (0.89)	6.78 (0.31)	8.63	7.14 (0.23)	7.19 (0.24)	6.91 (0.14)	6.89 (0.12)	8.27	6.54 (0.32)
P_2O_5	0.03 (0.02)	0.05 (0.02)	0.09	0.04 (0.02)	0.05 (0.03)	0.05 (0.03)	0.04 (0.02)	0.17	0.04 (0.02)
Cl	0.47 (0.08)	0.77 (0.05)	0.60	0.70 (0.07)	0.72 (0.04)	0.71 (0.02)	0.82 (0.02)	0.39	0.56 (0.07)
F	0.00 (0.00)	0.20 (0.16)	0.00	0.00 (0.00)	0.00 (0.00)	0.00 (0.00)	0.04 (0.03)	0.00	0.00 (0.00)
K_2O/Na_2O	2.29 (0.33)	1.21 (0.44)	1.79	1.23 (0.04)	1.24 (0.08)	1.19 (0.02)	1.09 (0.02)	2.10	1.22 (0.10)
Total $_{corr.}$	**96.69 (0.94)**	**98.87 (1.41)**	**98.73**	**97.76 (1.19)**	**97.13 (1.27)**	**97.04 (1.33)**	**98.08 (1.29)**	**98.14**	**98.79 (1.11)**

Table 3

Primary tephra layer	**Thickness (mm)**	**Sediment type***	**Reworked tephra material after primary tephra deposition**	**Increased diatom population after tephra deposition**	**Increased µ-XRF signal of primary tephra**
TM-17-2	20	L4	1-4 yrs intra-basin, up to >10yrs catchment	1^{st} –3^{rd} yr	K, Si, Ca
TM-18	230	L2/L3	1-8 yrs intra-basin, up to >1240 yrs catchment	1^{st} (3^{rd}) – 8^{th} yr	K
TM-18-1a	32	L1/L2	1 yr intra-basin, up to >70 yrs catchment	1^{st} – 3^{rd} yr	K
TM-18-1b	6	L1	Scattered and bioturbated up to 2 cm above tephra	Not visible	n.a.
TM-18-1c	5	L2	1-3 yrs intra-basin, up to 30 yrs catchment	2^{nd} – 3^{rd} yr	K, Mn
TM-18-1d	10	L2	1-2 yrs intra-basin, up to 62 yrs catchment	1^{st} – 10^{th} yr	K, Mn
TM-18-2	1	L2	up to 6 yrs catchment	-	n.a.

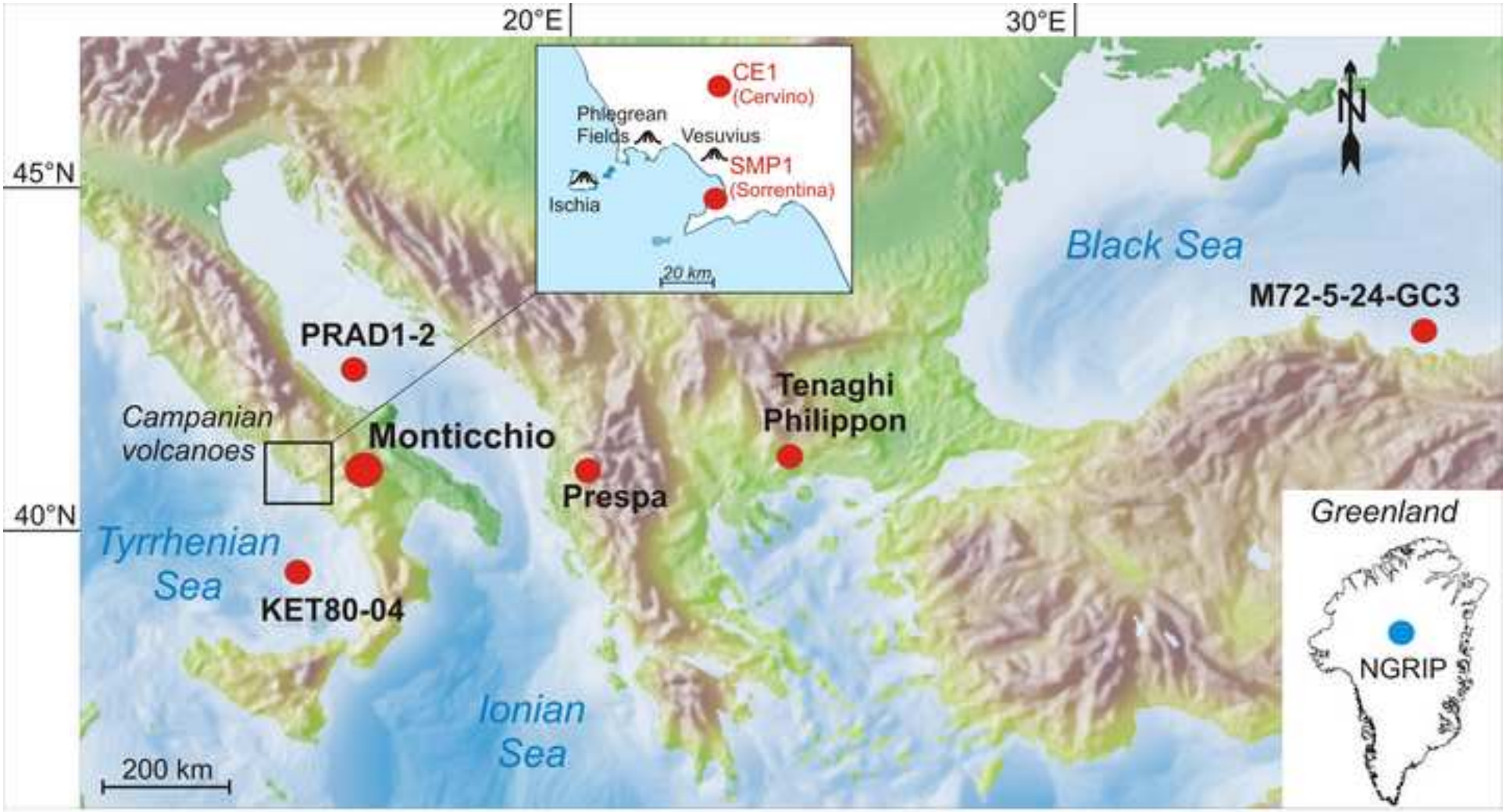
20°E
30°E
45°N
40°N
CE1
(Cervino)
Phlegrean
Fields
Vesuvius
SMP1
(Sorrentina)
Ischia
20 km
N
Black Sea
M72-5-24-GC3
PRAD1-2
Tenaghi
Philippon
Campanian
volcanoes
Monticchio
Prespa
Tyrrhenian
Sea
KET80-04
Ionian
Sea
200 km
Greenland
NGRIP

Figure 1

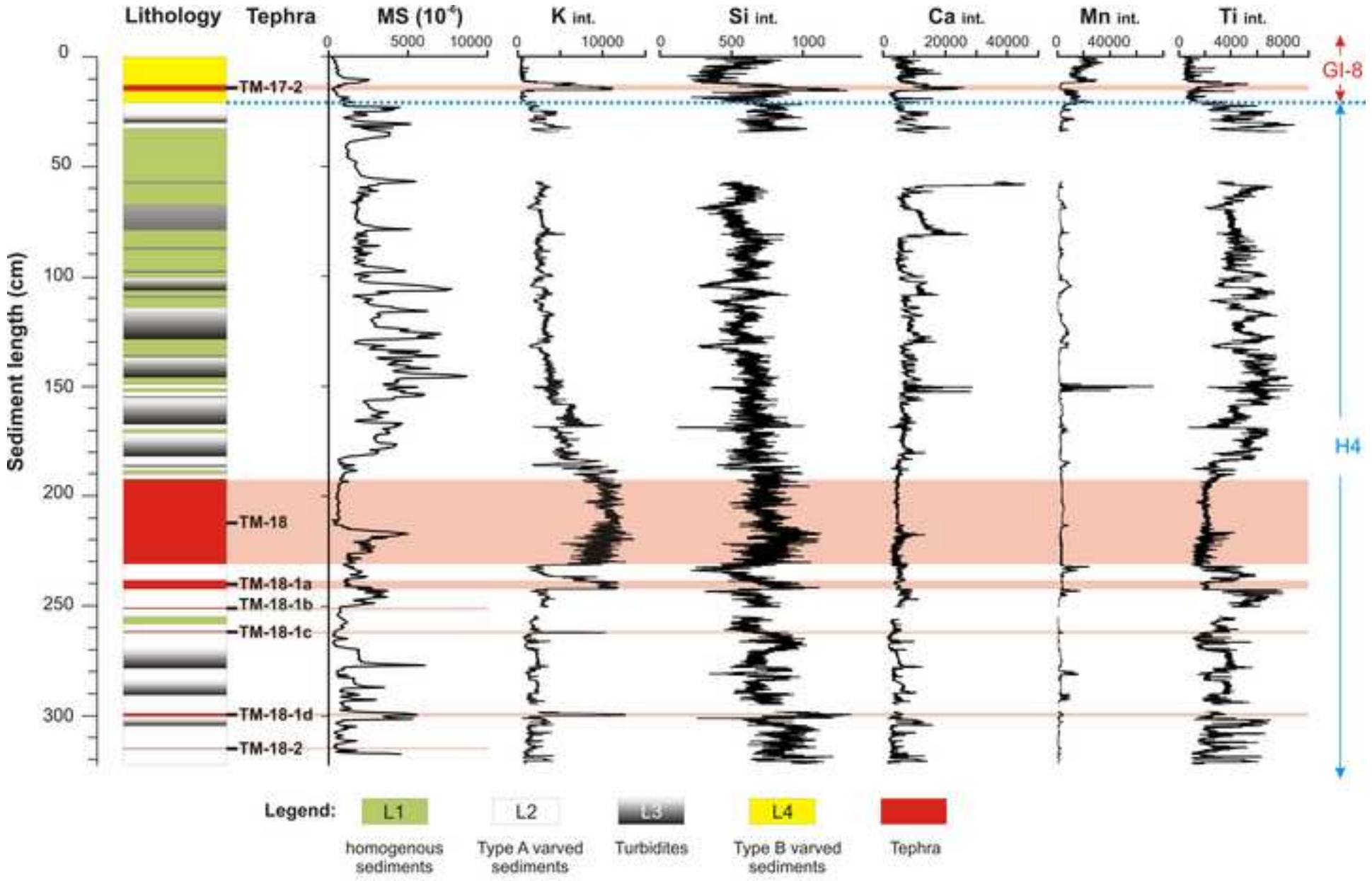
Lithology
Tephra
MS (10⁻⁶)
K int.
Si int.
Ca int.
Mn int.
Ti int.
0
5000
10000
0
10000
0
500
1000
0
20000
40000
0
40000
0
4000
8000
Sediment length (cm)
0
50
100
150
200
250
300
TM-17-2
TM-18
TM-18-1a
TM-18-1b
TM-18-1c
TM-18-1d
TM-18-2
GI-8
H4
Legend:
L1
homogenous sediments
L2
Type A varved sediments
L3
Turbidites
L4
Type B varved sediments
Tephra

Figure 2

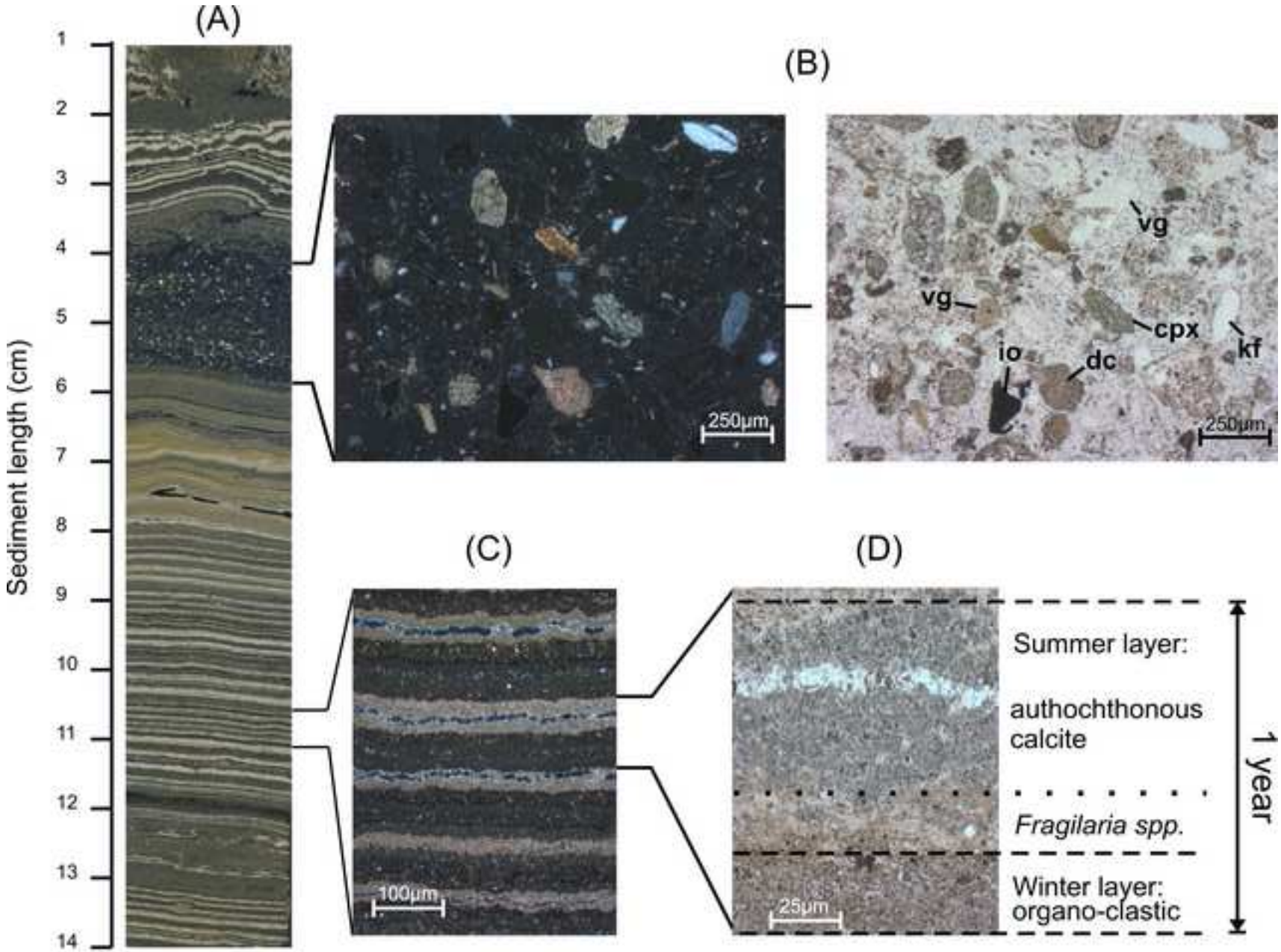
(A)
(B)
(C)
(D)
Sediment length (cm)
1
2
3
4
5
6
7
8
9
10
11
12
13
14
250µm
vg
vg
cpx
kf
io
dc
250µm
100µm
Summer layer:
authochthonous calcite
Fragilaria spp.
Winter layer:
organo-clastic
25µm
1 year

Figure 3

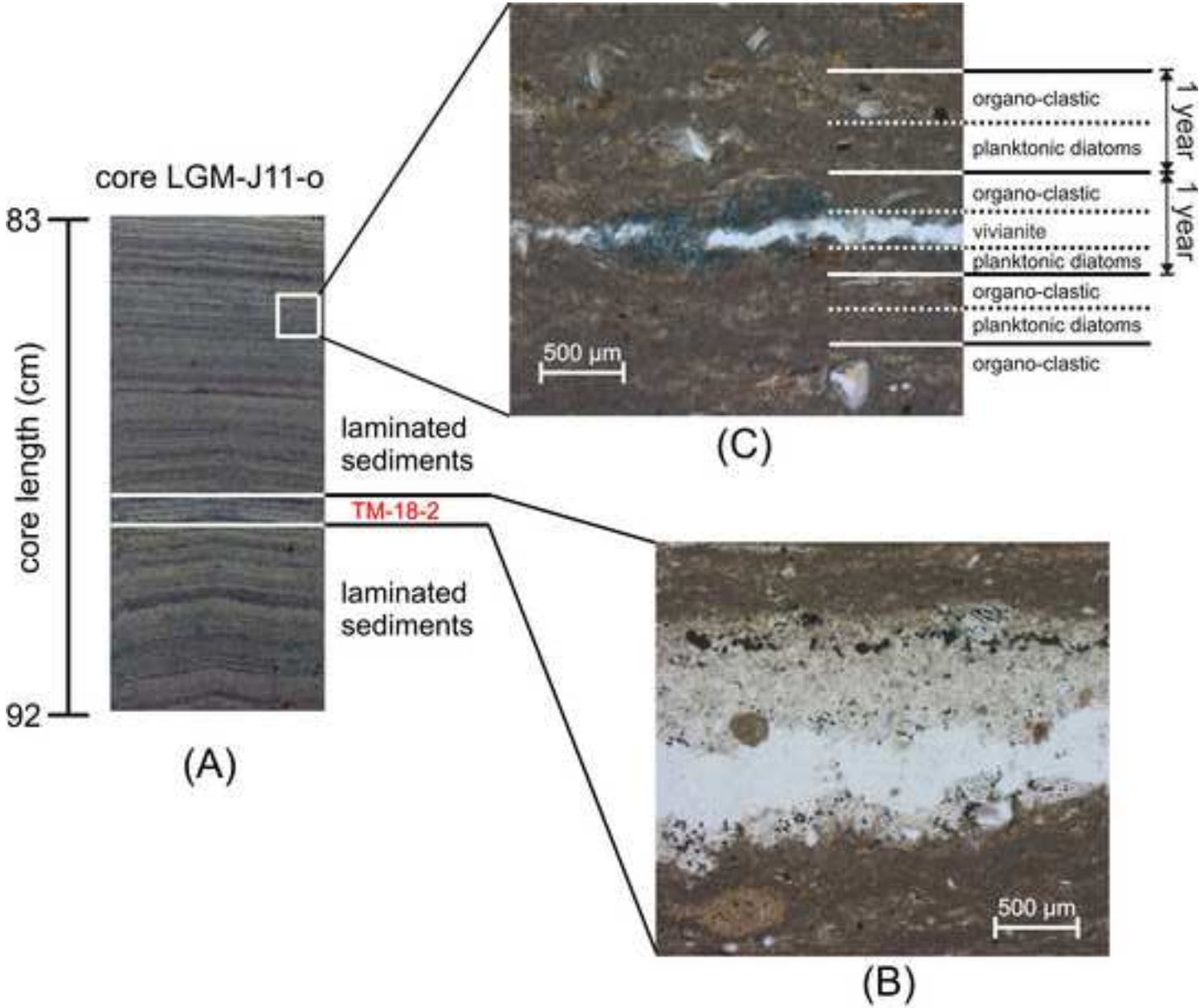
core LGM-J11-o
83
92
core length (cm)
laminated sediments
TM-18-2
laminated sediments
(A)
500 µm
organo-clastic
planktonic diatoms
organo-clastic
vivianite
planktonic diatoms
organo-clastic
planktonic diatoms
organo-clastic
1 year
1 year
(C)
500 µm
(B)

Figure 4

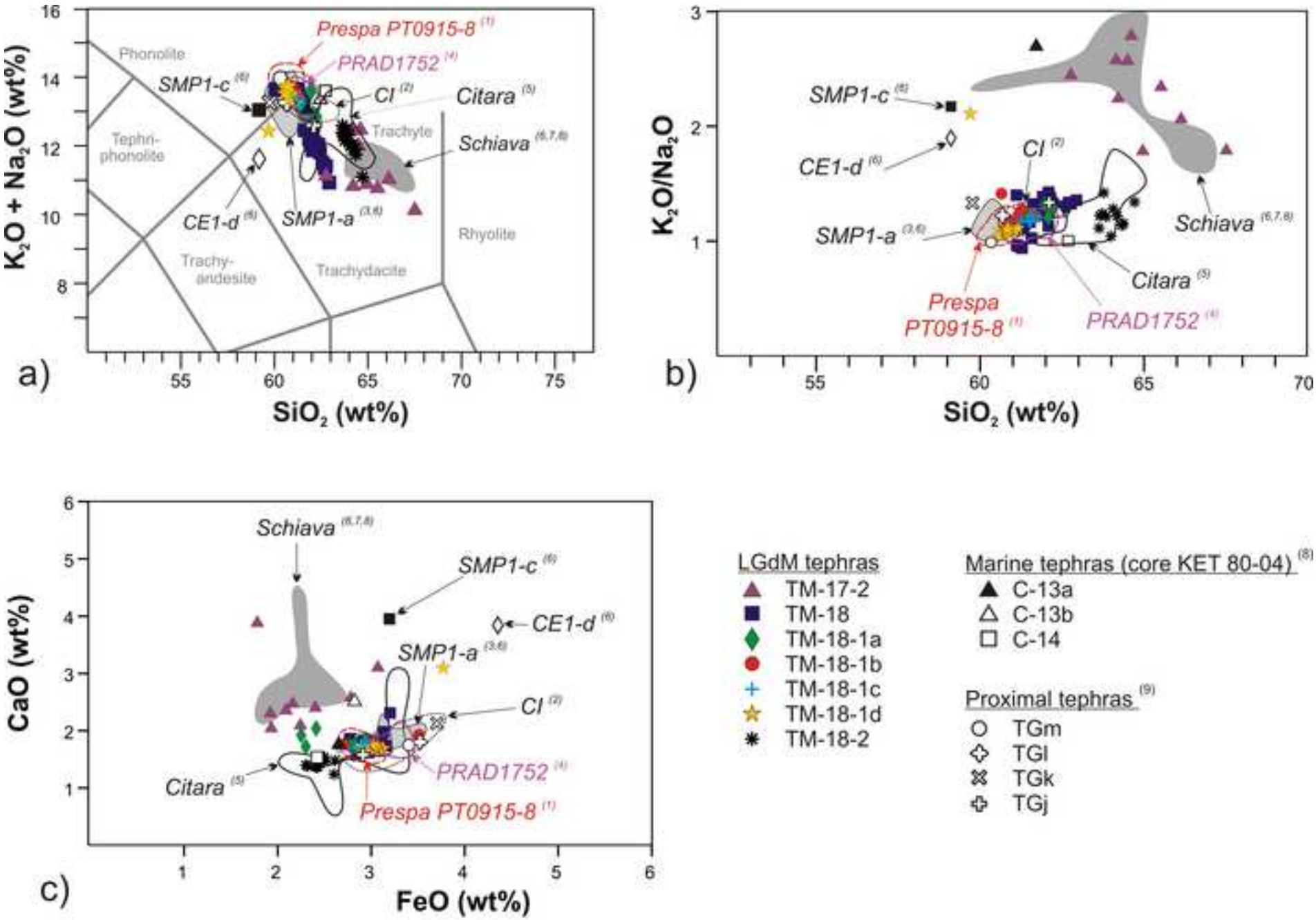
a)
$K_2O + Na_2O$ (wt%)
SiO_2 (wt%)
Phonolite
Tephri-phonolite
Trachyte
Rhyolite
Trachy-andesite
Trachydacite
Prespa PT0915-8 (1)
PRAD1752 (4)
SMP1-c (6)
CI (2)
Citara (5)
Schiava (6,7,8)
CE1-d (6)
SMP1-a (3,6)
b)
K_2O/Na_2O
SiO_2 (wt%)
c)
CaO (wt%)
FeO (wt%)
LGdM tephras
TM-17-2
TM-18
TM-18-1a
TM-18-1b
TM-18-1c
TM-18-1d
TM-18-2
Marine tephras (core KET 80-04) (8)
C-13a
C-13b
C-14
Proximal tephras (9)
TGm
TGl
TGk
TGj

Figure 5

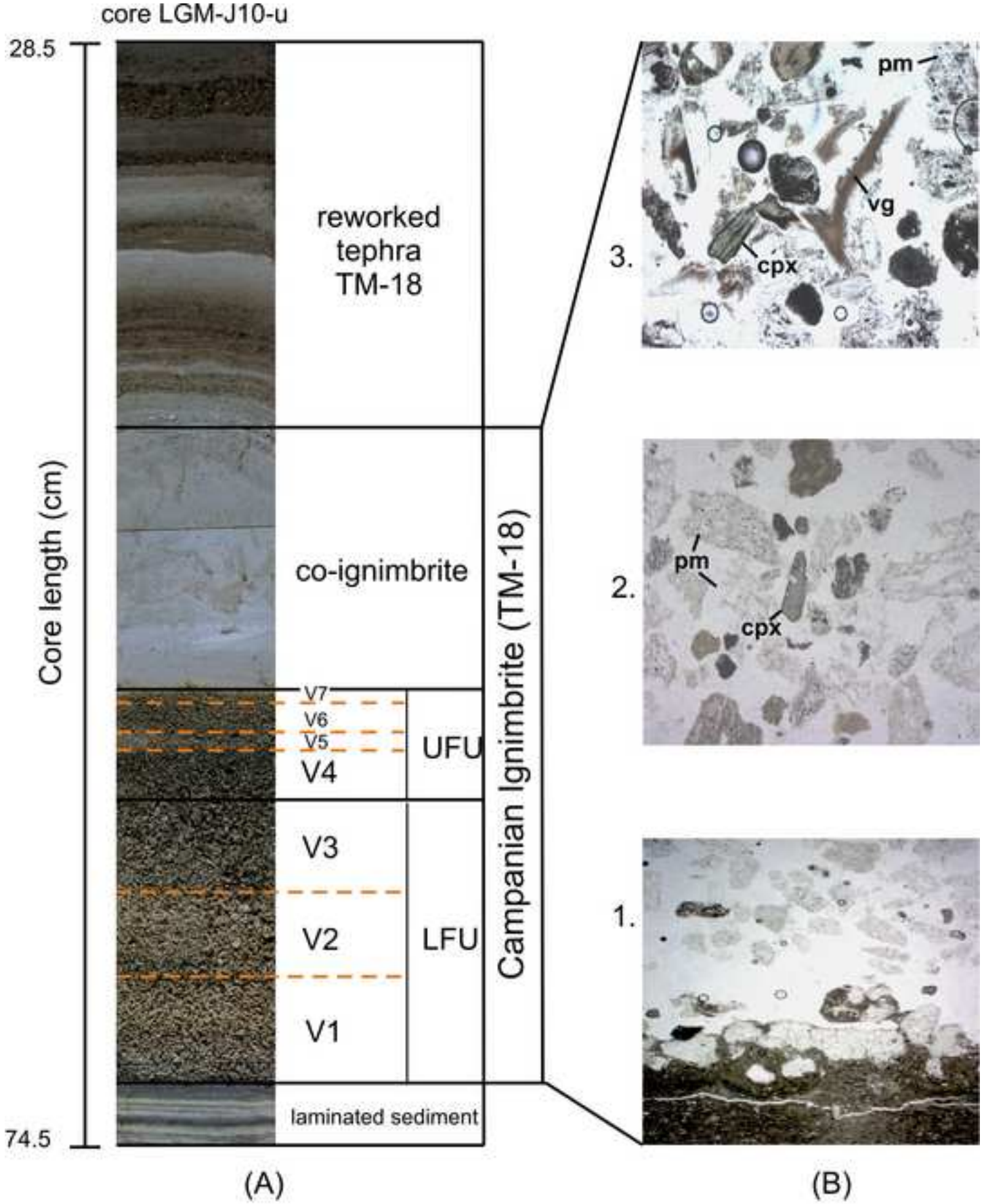
core LGM-J10-u
28.5
74.5
Core length (cm)
reworked
tephra
TM-18
co-ignimbrite
V7
V6
V5
V4
UFU
V3
V2
V1
LFU
laminated sediment
Campanian Ignimbrite (TM-18)
3.
pm
vg
cpx
2.
pm
cpx
1.
(A)
(B)

Figure 6

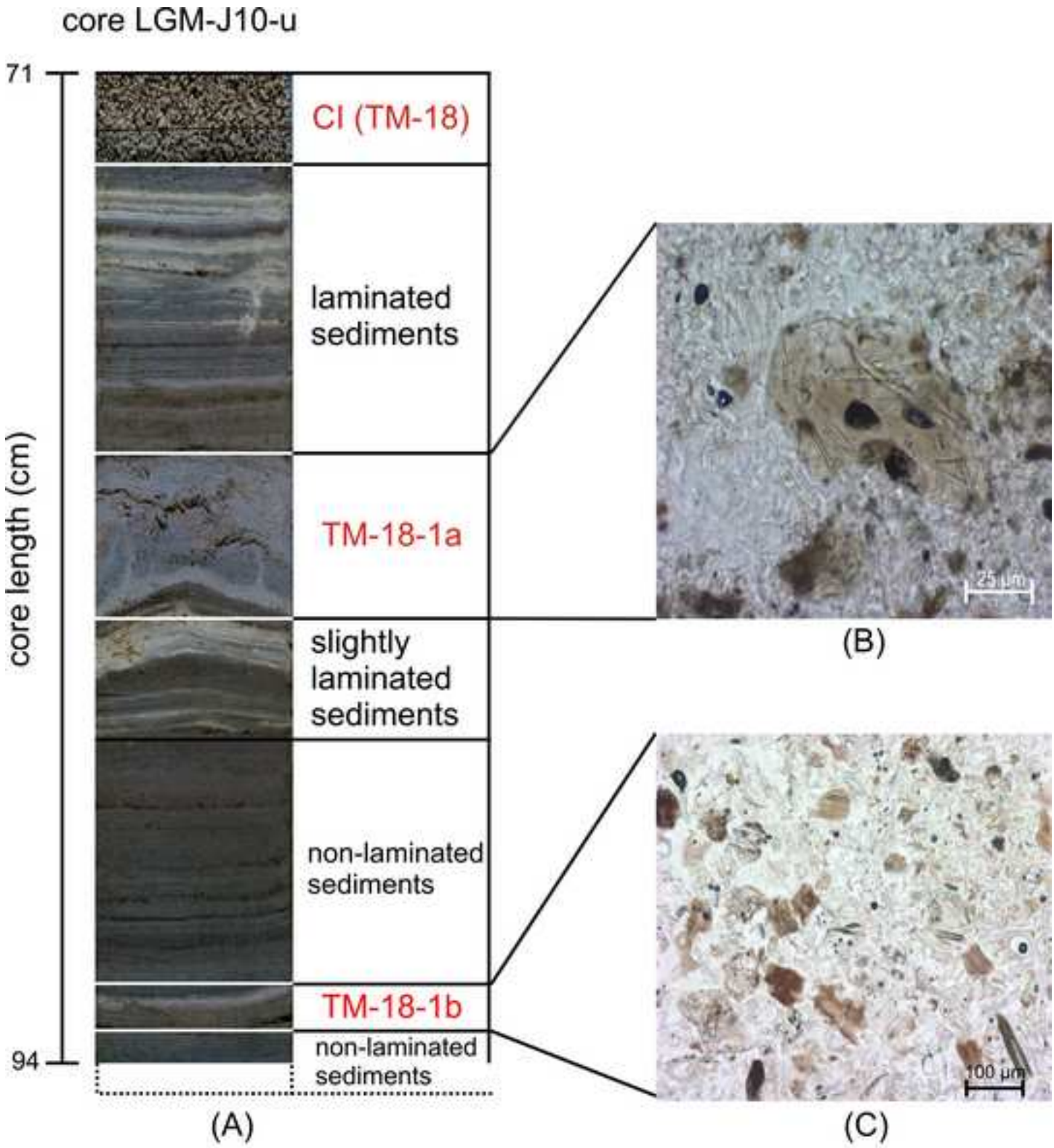
core LGM-J10-u
71
94
core length (cm)
CI (TM-18)
laminated sediments
TM-18-1a
slightly laminated sediments
non-laminated sediments
TM-18-1b
non-laminated sediments
(A)
25 µm
(B)
100 µm
(C)

Figure 7

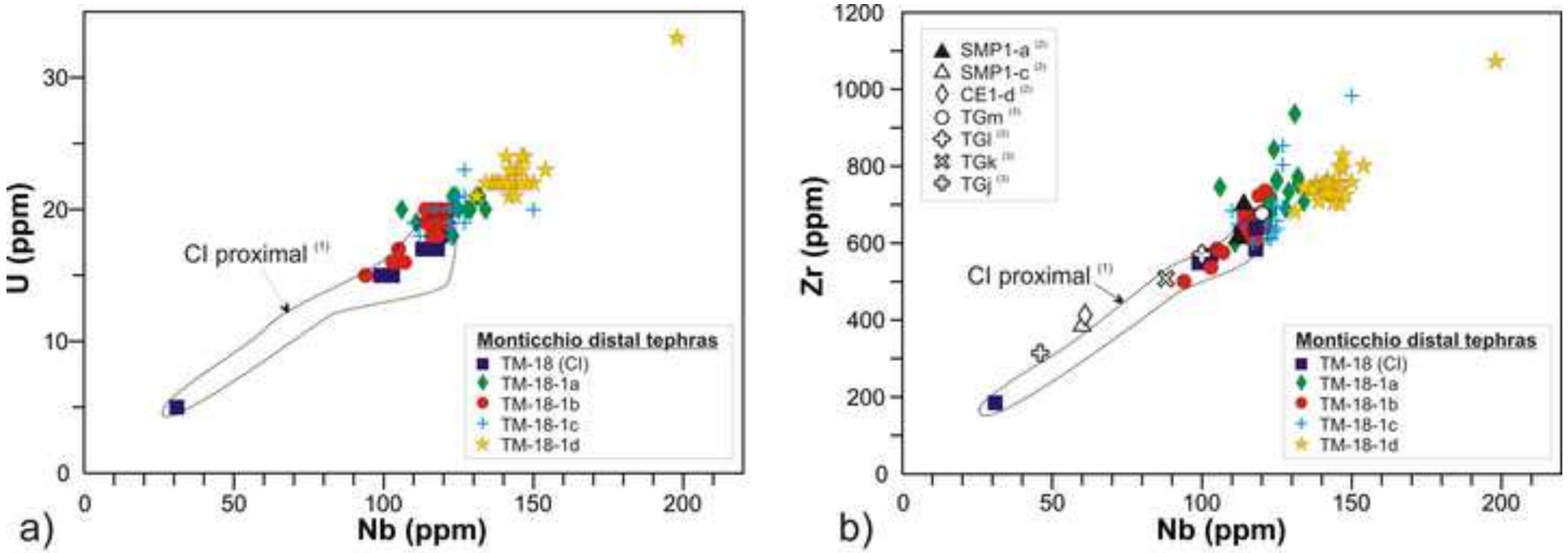
a)
U (ppm)
Nb (ppm)
CI proximal (1)
Monticchio distal tephras
TM-18 (CI)
TM-18-1a
TM-18-1b
TM-18-1c
TM-18-1d
b)
Zr (ppm)
Nb (ppm)
SMP1-a (2)
SMP1-c (2)
CE1-d (2)
TGm (1)
TGl (3)
TGk (3)
TGj (3)
CI proximal (1)
Monticchio distal tephras
TM-18 (CI)
TM-18-1a
TM-18-1b
TM-18-1c
TM-18-1d

Figure 8

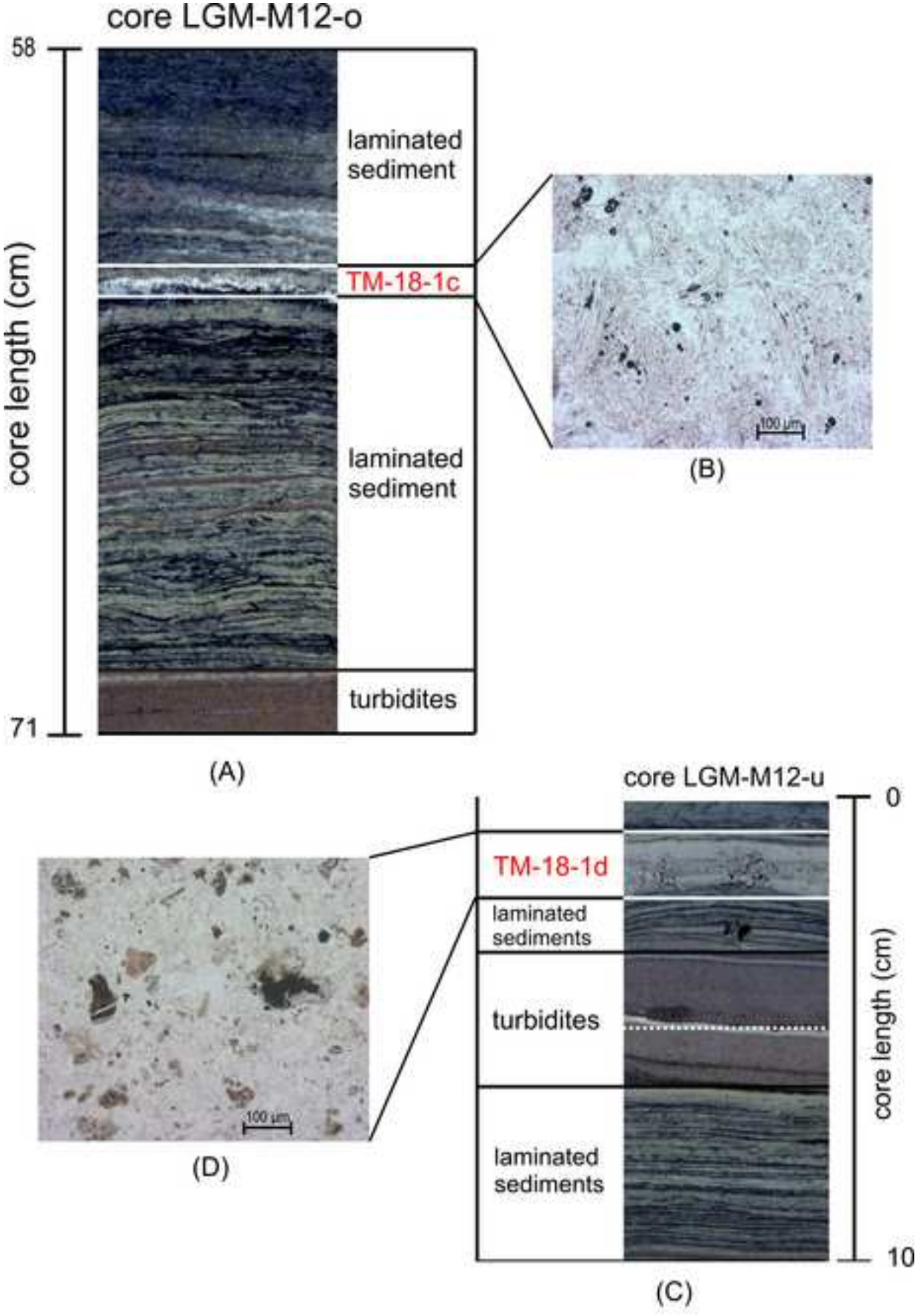
core LGM-M12-o
58
71
core length (cm)
laminated sediment
TM-18-1c
laminated sediment
turbidites
100 µm
(B)
(A)
core LGM-M12-u
0
10
core length (cm)
TM-18-1d
laminated sediments
turbidites
laminated sediments
100 µm
(D)
(C)

Figure 9

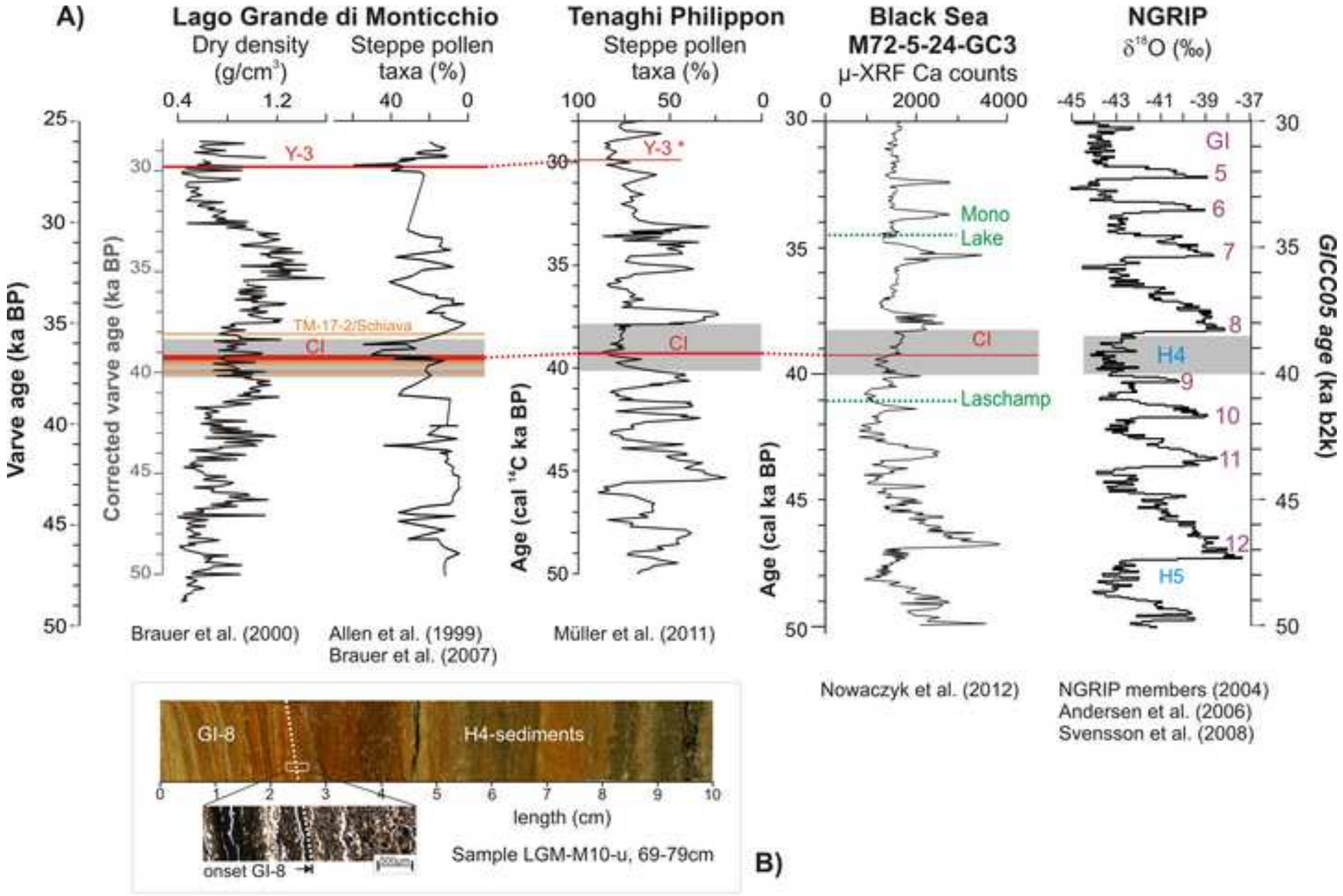
A)
Lago Grande di Monticchio
Dry density (g/cm³)
Steppe pollen taxa (%)
Tenaghi Philippon
Steppe pollen taxa (%)
Black Sea
M72-5-24-GC3
μ-XRF Ca counts
NGRIP
δ18O (‰)
Varve age (ka BP)
Corrected varve age (ka BP)
Age (cal ¹⁴C ka BP)
Age (cal ka BP)
GICC05 age (ka b2k)
Y-3
Y-3 *
TM-17-2/Schiava
CI
Mono Lake
Laschamp
GI
5
6
7
8
H4
9
10
11
12
H5
Brauer et al. (2000)
Allen et al. (1999)
Brauer et al. (2007)
Müller et al. (2011)
Nowaczyk et al. (2012)
NGRIP members (2004)
Andersen et al. (2006)
Svensson et al. (2008)
GI-8
H4-sediments
length (cm)
onset GI-8
Sample LGM-M10-u, 69-79cm
B)

Figure 10